Primordial nucleosynthesis: The effects of injecting hadrons

M. H. Reno
Fermi National Accelerator Laboratory, P.O. Box 500, Batavia, Illinois 60510

D. Seckel
Santa Cruz Institute for Particle Physics, University of California, Santa Cruz, California 95064
(Received 12 August 1987)

We place constraints on the abundance of quasistable particles with hadronic decay modes using the upper bounds on primordially produced ^{4}He and the sum of D and ^{3}He abundances. The results are presented as a function of particle lifetime (ranging between 10^{-1} and 10^4 sec), particle mass, and hadronic branching ratio. We apply our results to the cases of gravitinos, photinos in $\tilde{R}$-parity-violating theories, and mirror quarks. We also discuss another mechanism for hadron injection: cold-dark-matter annihilation.

I. INTRODUCTION

The agreement between big-bang nucleosynthesis (BBN) calculations and observations of light-element abundances provides a strong argument in favor of the standard big-bang cosmology.[1] The fact that agreement is attained at all is remarkable, even more so because small deviations of the input parameters ruin the good predictions of the standard cosmology. On this basis,[2] one may conclude that the number of light neutrino species N_ν is less than 5 and that the contribution of baryons to the closure density of the Universe Ω_B is less than 0.2. These two statements have profound effects on our view of particle physics and cosmology, particularly a prejudice for closure density $\Omega=1$, and ideas about dark matter.[3] Considerable effort has been made to see if these conclusions can be modified by additional hypotheses. Consequently, various authors have considered inhomogeneities in baryon number,[4] neutrino degeneracy,[5] neutrino masses,[6] entropy production,[7] photofission of light nuclei,[8–11] etc., as mechanisms for modifying standard BBN.

Instead of trying to alter some of the fundamental hypotheses in BBN calculations, one may use the consistency of BBN with observations as a constraint on variations of standard cosmology or standard particle physics. This is the approach we take. Our objective in this work is to assess the effects on BBN of injecting strongly interacting particles during nucleosynthesis. We place constraints on the mass, lifetime, and primordial abundance of any hypothetical unstable particles, denoted by X, that decay into quarks or gluons. Examples of decaying particles are gravitinos that decay into gluon-gluino,[11,12] photinos in theories where $\tilde{R}$ parity is violated,[10,13] and quasistable quarks such as those occurring in O(18) models.[14] We also discuss cosmological models dominated by cold-dark-matter[15] particles of a few-GeV mass where dark-matter annihilations produce hadrons. Some of the effects considered here have been discussed by Dominguez-Tenreiro[11] for the case of gravitino decay and more generically by Dominguez-Tenreiro and Yepes.[16] In addition, recently Dimopoulos, Esmailzadeh, Hall, and Starkman[17] (DEHS) have embarked on an ambitious program to explore the possibility of $\Omega_B=1$ in models where X decays around 10^5–10^6 sec.

The effects we are considering are easy to describe qualitatively. Suppose a 100-GeV X particle decays producing some energetic quarks or gluons. Each quark or gluon results in a jet of strongly interacting particles, i.e., mesons, baryons, and antibaryons. These particles may decay, but the longer-lived species have a chance to interact with the ambient protons and neutrons. When these interactions take place, there is a significant probability that the target nucleon will change isospin, i.e., $p\rightarrow n$ or vice versa. The calculated light-element abundances depend on the neutron density. By requiring these abundances to remain within observational bounds, we can work backwards to derive a limit on how many X decays are allowed during the nucleosynthesis era.

There are four temperature regimes, each manifesting different effects due to the injection of hadrons. When $T\gtrsim 0.7$ MeV, proton-neutron interconversion through weak interactions largely washes out the effects of hadronic conversion of protons and neutrons. The equilibrium ratio of neutrons to protons is preserved except for large hadronic injection rates at temperatures above 0.7 MeV.

When weak charge-exchange reactions "freeze-out" at a temperature $T\sim 0.7$ MeV the fraction of baryons found in neutrons x_n is ~ 0.16. Because of neutron β decay, x_n decreases to ~ 0.12 by the time the "deuterium bottleneck" breaks at $T\sim 0.08$ MeV and nucleosynthesis of the light elements proceeds. The major effect of injecting strongly interacting particles when $0.7\gtrsim T\gtrsim 0.08$ MeV is to induce $p\rightarrow n$ reactions because there are more target protons than target neutrons. The extra neutrons produced in this way result in an enhanced helium abundance Y.

When $T\lesssim 0.08$ MeV, the deuterium abundance first increases then decreases as the neutrons are processed into helium. Before $T\sim 0.05$ MeV, most neutrons end up in ^{4}He. For $T\lesssim 0.05$ MeV, there are no free neutrons left in

the standard model of BBN. Furthermore, the deuterium (D) left over from nucleosynthesis is so dilute that it no longer burns into heavier isotopes via ^{3}He and tritium (T). Strongly interacting particles injected at this time induce $p \rightarrow n$ reactions and result in free neutrons that bind into deuterium. Since the deuterium does not burn, the major effect here is to increase the deuterium abundance. Although it is less obvious, the free neutrons also have a significant effect on the ^{7}Li abundance. In addition to inducing $p \rightarrow n$ reactions, antibaryons and/or high-energy neutrons may induce fission of ^{4}He. This acts as another source of n, D, T, and ^{3}He. We have not calculated these effects carefully and present results as if they did not occur. Because they can only increase the abundance of deuterium, and our constraints in this time range are based on an overproduction of D, we have been overly conservative.

Finally, there is a fourth regime ($T \lesssim 3$ keV) when the neutrons released by strong interactions decay before they can bind into deuterium. The major effect of injecting strongly interacting particles in this regime is due to the fractional probability for ^{4}He to suffer induced fission into ^{3}He, T, or D (Refs. 11 and 12). Unless this fraction is very small, the overabundance of ^{3}He, T, and D produced by the fission of ^{4}He is much more significant than the decrease in ^{4}He. For $T \lesssim 3$ keV, one should also take into account the photofission of light nuclei.[8–11,17] It is important to realize that photofission may act to deplete deuterium for $10^4 \lesssim t \lesssim 10^6$ sec, and this would weaken our bounds. We did not include photofission and so confine our analysis to time scales less than 10^4 sec.

At this stage we would like to clarify a few conceptual points. The first point pertains to charge symmetry. Although the injection spectrum and individual cross sections may be charge symmetric, the target medium definitely is not. As we have already remarked, the neutron fraction ranges from 0.5 to 0.12. A net charge flow $p \rightarrow n$ is induced upon a charge-symmetric, out-of-equilibrium, introduction of strongly interacting particles whenever $x_n < 0.5$. Actually, the cross sections are not precisely charge symmetric due to mass differences within isospin multiplets. In fact, it is just this sort of mass difference ($m_n - m_p \simeq 1.3$ MeV) that leads to the original asymmetry of the medium. We emphasize, however, that even with charge-symmetric cross sections in the calculation, a net charge flow is induced.

The second point regards the treatment of injected baryons and antibaryons. We begin by supposing X decays with no net baryon number, e.g., the number of neutrons equals the number of antineutrons in the final state. Even though they are not physically bound together we can think of them being injected and interacting in pairs: $(n\bar{n})+n \rightarrow n \cdots$ or $(n\bar{n})+p \rightarrow n \cdots$. In this way we treat baryon-antibaryon pairs the same way we would very long-lived mesons, i.e., their only effect is to induce $p \leftrightarrow n$ interactions. On the other hand, when X carries baryon number, we modify the discussion to account for a net change in baryon number.

Finally, we comment on interaction times versus decay times. It is clear that for baryon-antibaryon pairs, hadronic interaction times are short compared to decay times. For mesons, surprisingly, the two time scales are competitive. The baryon density is large enough at $T \sim 1$ MeV for meson-baryon strong-interaction rates to compete with meson decay rates, so the ^{4}He abundance is affected. In regard to interaction rates, the interactions of interest are exothermic, so the cross section times relative velocity is constant at low energies, rather than going to zero. However, by the time the Universe cools to 0.1 MeV, the baryon density is too low for mesons to make a significant change in light-element abundances.

We have sketched the effects of injecting hadrons during nucleosynthesis. The rest of this paper provides more details. In Sec. II we quickly review standard BBN and the observational limits on light-element abundances. In Sec. III we describe how we modify standard BBN calculations to account for strongly interacting particles. This is where we give the cross sections, particle multiplicities, etc., that provide the details of our analysis. Section IV contains the bulk of our results concerning injection due to decaying particles. Section V has a discussion of the injection of strongly interacting particles due to the annihilation of cold dark matter. Finally, Sec. VI contains a summary of our results and a discussion of the uncertainties in our calculations.

II. STANDARD BIG-BANG NUCLEOSYNTHESIS

We briefly review the standard picture of big-bang nucleosynthesis, with an eye towards how the standard results change upon injecting hadronic matter. First, we repeat the quantitative analysis of previous authors and give qualitative reasons for why the light-element abundances behave as they do. This framework allows us to understand in a general way the detailed results to follow in Secs. IV and V. We state here our choices for observational limits on light-element abundances.

The standard model of BBN has been discussed extensively in the literature.[18] Using nuclear and electroweak interaction rates in a homogeneous and isotropic Universe, the dynamical evolution of nucleon and nuclear densities can be traced as a function of the temperature of the Universe. The parameters that enter into the calculation of the final abundances of light elements include the number of light neutrinos N_ν, the neutron half-life $\tau_{1/2}$, and the baryon-to-photon number density ratio η. Throughout, we set N_ν to 3. We fix the neutron half-life at the Particle Data Group[19] central value of $\tau_{1/2} \simeq 10.4$ min. The error quoted is of order 0.2 min. Traditionally, the elemental number densities are normalized by the number density of hydrogen, e.g., $X_{\rm D} = n({\rm D})/n({\rm H}) \equiv ({\rm D}/{\rm H})$, except for ^{4}He which is normalized to the total mass density, $Y = 4X_{^4{\rm He}}/(1+4X_{^4{\rm He}})$. Sometimes we show abundances normalized to entropy, $y_X \equiv n_X/s$. To arrive at the final values of the light-element abundances, the equations of nuclear and nucleon reaction kinetics are solved. In practice, the equations are numerically integrated. For our presentation here, we use the Wagoner computer code.[20]

Figure 1 shows the standard-model results for (a) ^{4}He, (b) ^{3}He and D, and (c) ^{7}Li, as a function of baryon density. The qualitative features of these graphs are under-

stood. The critical quantity is the time t_D when the rate for deuterium burning exceeds that for deuterium photofission. This "deuterium bottleneck" breaks at a few hundred seconds. Before t_D, essentially all baryons are in single nucleons, protons, or neutrons; but as soon as deuterium accumulates, the rest of the nuclear reactions quickly cook almost all neutrons into ^{4}He, the most tightly bound of the light elements. Nuclear burning is not completely efficient so residual numbers of other light elements account for a small fraction of the neutrons.

From this argument, we see that the helium abundance is determined by the neutron abundance at the time the deuterium bottleneck breaks. That is, $Y \simeq 2x_n$ where x_n is the fraction of baryons in neutrons just before t_D. For times between a few seconds and a few hundred seconds, the only weak interactions operative are neutron β decays so $x_n \sim e^{-t_D/\tau_n}$. We can now understand why in Fig. 1, Y is fairly insensitive to η. The rate for photofission of D is controlled by the number density of photons with energy greater than the binding energy of D, $E_\gamma > E_D = 2.2$ MeV. For $T \ll E_D$, the rate for photofission depends exponentially on the photon temperature T through the Boltzmann factor $e^{-E_D/T}$. Increasing the baryon density and thus the formation rate of D requires a small logarithmic change to t_D to increase the effective photon density. This in turn results in a logarithmic increase in x_n and Y.

Contrary to the ^{4}He abundance, the other light-element abundances show large variations with η. Part of this variation is due to the choice of normalization. Because the abundances are measured relative to hydrogen, for a constant element abundance, as η increases, $X_i \sim 1/\eta$. However, the absolute abundances are not constant. For higher η, the neutron density drops sooner and faster. As a result, reactions involving neutrons turn off sooner at higher η. We briefly look at these two effects on D, T, ^{3}He, and ^{7}Li.

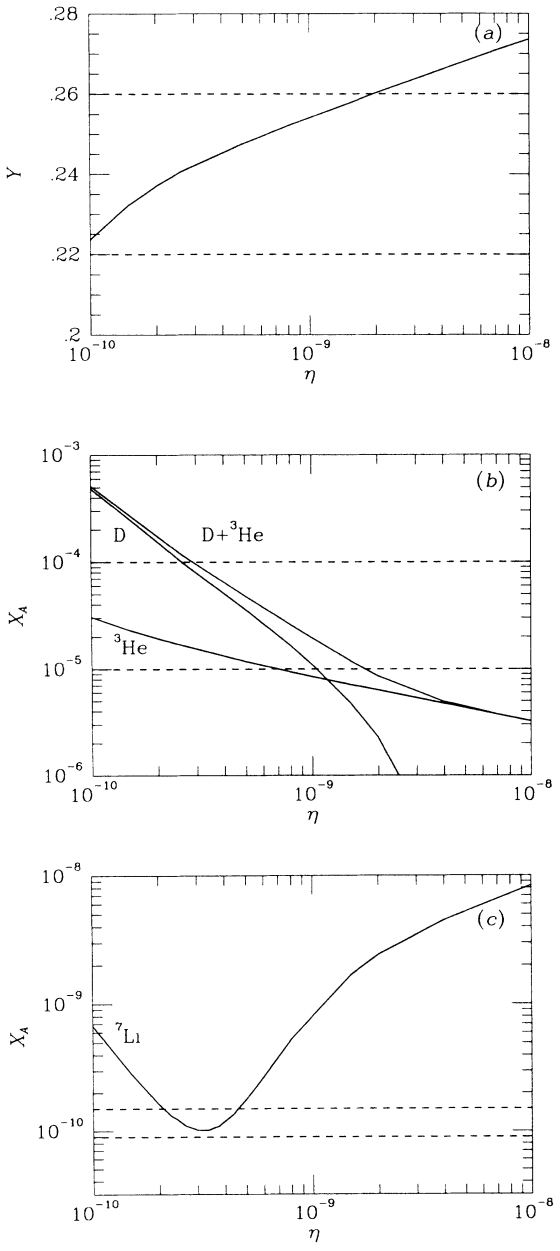

FIG. 1. Standard-model results for (a) ^{4}He, (b) ^{3}He and D, and (c) ^{7}Li as a function of η, the present baryon to photon density ratio.

A. D

Immediately following the breaking of the deuterium bottleneck, there is a brief period of time where the fuel source for nucleosynthesis is neutrons. The neutron number drops exponentially and soon that fuel source is exhausted. There then ensues a stage wherein deuterium production has stopped and deuterium is the consumable resource. For most of this period D is consumed by DD$\rightarrow n\,^3$He,pT reactions.

When the abundance of a species is determined by reactions with two particles of species a in the initial state, the final abundance y_f is generally insensitive to the initial abundance. Rather $y_f \sim x/C$; where $x = m_a/T_i$, $C \propto \sigma_{aa}$ is a constant proportional to the reaction cross section,[21] and T_i is the temperature below which the production of the species a is unimportant. For a = D, this is when the neutron fuel is exhausted.

If the initial values of T_i and σ_{aa} were independent of η then the absolute final abundance of D would be η independent and therefore $X_D \sim 1/\eta$. In fact, for higher values of η the neutron number drops faster so the initial time for DD burning to dominate occurs earlier. This implies a higher value of T_i which in turn implies a higher cross section because it is easier to overcome the DD Coulomb barrier. Both these increases result in decreasing the final value of x, so as a result X_D falls faster than $1/\eta$. For very high values of $\eta \gtrsim 10^{-9}$, DD reactions deplete D to the point where the dominant D reaction is D$p \rightarrow \gamma\,^3$He. When this happens D falls very quickly with η, as increasing η increases the "optical depth" of the Universe to deuterium.

B. T

The tritium abundance is easily understood as competition between the dominant formation ($DD \rightarrow pT$) and destruction reactions ($DT \rightarrow n\,^4He$). This fixes $X_T \simeq (\sigma_{DD\rightarrow pT}/\sigma_{DT\rightarrow n^4He})X_D$, or $X_T \simeq 10^{-2}X_D$. The lifetime of T is 3.9×10^8 sec and T decays to ^{3}He so the final abundance of ^{3}He is slightly enhanced.

C. ^{3}He

The ^{3}He abundance is complicated by the reactions $n\,^3He \rightarrow pT$ and $Dp \rightarrow \gamma\,^3He$. Until $x_n \lesssim X_D/10$, the neutrons keep $X_{^3He}$ from rising to trace the rise of X_D. Later, during D burning, the neutrons produced in $DD \rightarrow n\,^3He$ may recombine with ^{3}He. This reaction also suppresses $X_{^3He}$ relative to X_D. However, in the late stages of D burning, the neutrons may decay so that the ^{3}He produced remains. This provides for an increase in $X_{^3He}$ as η decreases. For high η (low X_D, so that DD burning is less important), $X_{^3He}$ tends to a value ($\sim 3\times10^{-6}$) determined by the ratio of the Dp and $D\,^3He$ cross sections.

D. ^{7}Li

The final value of $X_{^7Li}$ is actually the sum of the mass 7 nucleides ^{7}Li and ^{7}Be which eventually electron captures to form ^{7}Li. ^{7}Li is primarily formed by $T\,^4He \rightarrow \gamma\,^7Li$ and destroyed by $p\,^7Li \rightarrow 2\,^4He$. Similarly, ^{7}Be is formed by $^3He\,^4He \rightarrow \gamma\,^7Be$ but is destroyed by $n\,^7Be \rightarrow p\,^7Li$. In low-$\eta$ models neutrons remain abundant enough after the high Coulomb barrier of the $^3He\,^4He$ reaction turns off ^{7}Be formation, so that most ^{7}Be is transformed into ^{7}Li. The Coulomb barrier for $T\,^4He$ is lower so the ^{7}Li abundance is determined by competing $T\,^4He$ and $p\,^7Li$ reactions. As a result, for $\eta \lesssim 3\times10^{-10}$, the ^{7}Li abundance traces the T and therefore the D abundances. For high η, the neutrons disappear earlier and there is no way to get rid of the ^{7}Be. The direct ^{7}Li production still traces T and D and so drops with increasing η. As a result $X_{^7Li}$ is dominated by ^{7}Be which increases with η as neutrons are eliminated earlier. The combination of low and high η arguments leads to the well-known minimum for $X_{^7Li}$ at $\eta \simeq 3\times10^{-10}$.

E. Observational limits

There are several reviews of the current status of observational studies of the light-element abundances.[2,22] We simply quote here the values used in the ensuing analysis. All of the limits appear as dashed lines in Figs. 1(a)–1(c). For the primordial abundance of ^{4}He, we take the conservative upper bound

$$Y_p \leq 0.26 \ . \tag{2.1a}$$

This is equivalent to using a 5σ uncertainty in the result of Kunth and Sargent,[23] $Y_p = 0.245 \pm 0.003$. Although our results are not sensitive to it, at one point in our analysis, we use a lower bound of $Y_p \geq 0.22$.

Deuterium is processed by stars into ^{3}He, so the primordial abundance is larger than the presently observed abundance:

$$(X_D)_p \geq (X_D)_o \gtrsim 10^{-5} \ . \tag{2.1b}$$

According to the stellar combustion argument, an upper bound on the sum of primordially produced D and ^{3}He is fairly model independent. A conservative upper bound is

$$(X_D + X_{^3He})_p \lesssim 10^{-4} \ . \tag{2.1c}$$

Henceforth, we drop the subscript p and refer only to primordial abundances.

The abundance of ^{7}Li observed in metal-poor stars is[24]

$$X_{^7Li} = (1.2 \pm 0.3)\times10^{-10} \ ; \tag{2.1d}$$

however, there is some debate as to whether or not this is indeed a measurement of the primordial ^{7}Li abundance or perhaps a consequence of galactic or stellar evolution. We do not use ^{7}Li to constrain decaying X particles, but we keep track of how their decay affects $X_{^7Li}$ (Ref. 25).

The dashed lines indicating the limits for ^{4}He, ^{3}He, and D can be used in the conventional scenario to fix the range of allowed values of η. The upper bound on $X_D + X_{^3He}$ puts $\eta \gtrsim 3\times10^{-10}$. The upper bound on Y requires $\eta \lesssim 2\times10^{-9}$. By also considering the lower bound on X_D, the maximum η value can be lowered to 10^{-9}. The range of $\eta \simeq (3-10)\times10^{-10}$ coincides with the range of estimates considered "conservative" by Yang *et al.*[2]

Deviations from the standard BBN model may allow for a larger range of η. By introducing X particles decaying into hadrons between $0.1-10^4$ sec, we find that the sum of the D and ^{3}He abundances is never decreased from the standard-model result for a given η. Therefore, we only consider $\eta \gtrsim 3\times10^{-10}$.

III. CHANGES TO NUCLEOSYNTHESIS DUE TO INJECTED HADRONS

In this section we itemize the changes to the equations governing nucleosynthesis, due to the injection of hadrons. For the most part this involves calculating the rate at which $p \leftrightarrow n$ transitions are induced by X decays. In cases where X carries baryon number B we must look at the effects of changing B during nucleosynthesis.

The transition rate for a nucleon N to convert to a nucleon of type $N' \neq N$ is comprised of two terms:

$$\Gamma_{N\rightarrow N'} = \Gamma^W_{N\rightarrow N'} + \Gamma^H_{N\rightarrow N'} \ , \tag{3.1}$$

where $\Gamma^W_{N\rightarrow N'}$ is the transition rate due to weak interactions, e.g., $e^- p \rightarrow \nu_e n$, and $\Gamma^H_{N\rightarrow N'}$ is the induced hadronic transition rate. The latter is given by the rate of X decays per N multiplied by the average number of $N \rightarrow N'$ transitions per X decay, denoted by $\mathcal{N}_{N\rightarrow N'}$. In terms of the decay rate for X particles $\Gamma_X = (\tau_X)^{-1}$, the number densities of X particles and baryons scaled by the entropy density, $y_X \equiv n_X/s$ and $y_B \equiv n_B/s$, and the fraction of baryons that are protons x_p and neutrons x_n, the rates $\Gamma^H_{N\rightarrow N'}$ are

$$\Gamma^H_{p\to n}=\frac{\Gamma_X y_X}{x_p y_B}\mathcal{N}_{p\to n},\quad \Gamma^H_{n\to p}=\frac{\Gamma_X y_X}{x_n y_B}\mathcal{N}_{n\to p}\ . \tag{3.2}$$

The average number of $N\to N'$ transitions is conveniently split into two factors:

$$\mathcal{N}_{N\to N'}=\sum_i P_{Xi} f^i_{NN'}\ , \tag{3.3}$$

where the sum is over the hadronic species that may be produced per X decay. The first factor P_{Xi} is the average number of species i in the final state from one X decay. This depends on branching ratios for various decay modes of X, fragmentation of partons into jets, and the mass of the X particle m_X. The second factor $f^i_{NN'}$ is the probability that hadron species i induces a transition $N\to N'$. This is strongly dependent on the environment of the decay, primarily because $f^i_{NN'}$ depends on nucleon number densities.

The transition probability $f^i_{NN'}$ can be expressed as the ratio of the absorption rate for $iN\to N'+\cdots$ compared to the sum of the i decay rate Γ^i_D and the *total* absorption rate Γ^i_A:

$$f^i_{NN'}=\frac{\Gamma^i_{NN'}}{\Gamma^i_D+\Gamma^i_A}\ . \tag{3.4}$$

The rate for strong interactions of meson i and nucleon N from the background medium is

$$\Gamma^i_{NN'}=9.6\times10^4 s_*(T)\frac{\eta}{10^{-10}}\left[\frac{T}{1\text{ MeV}}\right]^3 \times x_N\frac{\langle\sigma\beta\rangle^i_{NN'}}{1\text{ mb}}\ \text{sec}^{-1}\ , \tag{3.5}$$

where x_N is the density ratio of target nucleon N to the baryon density, $s_*(T)$ decreases from 2.75 to 1.0 to account for the change in n_B/n_γ as e^+e^- annihilation proceeds, and $\langle\sigma\beta\rangle$ is the strong-interaction cross section times velocity averaged over the thermal distribution of target nucleons. We have suggested in Sec. I, and we describe in more detail below, that baryon-antibaryon pairs can be treated as mesons, so Eq. (3.5) is applicable to the case where $i=n\bar{n},p\bar{p}$ as well.

As the typical value for strong-interaction cross sections is on the order of 1 mb, from Eqs. (3.4) and (3.5) we see that two types of hadronic particles have a chance of modifying nucleosynthesis. The first type are the long-lived mesons, $\pi^\pm$, $K^\pm$, and K_L, which have lifetimes of order 10^{-8} sec. For temperatures greater than about 1 MeV, the strong-interaction rate is competitive, or at least non-negligible, compared to the decay rate. These long-lived mesons therefore may affect the neutron-proton ratio at the time (and just after) it is being fixed by weak interactions. The second type of particle is nucleons and antinucleons. Throughout most of the range of temperatures considered here, neutrons and antineutrons have lifetimes much longer than their interaction times. Of course protons and antiprotons are stable so their interactions are always important throughout nucleosynthesis.

A. Thermalization

In order to evaluate the thermally averaged cross sections, we need to know the initial state of the hadron. For the most part, the injected particles "thermalize," i.e., they reach kinetic equilibrium with the medium before they interact with baryons in the medium, so the relevant $\langle\sigma\beta\rangle$ are for when both initial particles come from thermal distributions. Thermalization proceeds via scattering with electrons, positons, and photons in the medium. We leave a detailed discussion of thermalization times to the Appendix but summarize our conclusions here.

We begin with the charged mesons. Anticipating the results of Sec. IV, the charged mesons are important only for $T\gtrsim m_e$. In general, cross sections with electrons are larger than photon cross sections by a factor of $(m_i/T)^2$, where m_i is the hadron mass. Consequently, as long as e^+e^- are sufficiently abundant, that is, until $T<0.05m_e$, the Coulomb cross section dominates the thermalization rate. In the Appendix we show that the thermalization time for charged particles due to Coulomb scattering off of a relativistic e^+e^- gas is $\tau\sim10^{-14}(E/\text{GeV})(T/\text{MeV})^{-2}$ sec, where E is the initial energy of the hadron. Clearly, charged mesons thermalize since this time is much less than a hadronic interaction time which is always $\gtrsim10^{-8}$ sec.

Since (anti)protons are stable, we must consider thermalization at late times as well. Coulomb stopping dominates until $T\sim0.04m_e=0.02$ MeV. Inverse Compton scattering is efficient until $T=0.03$ MeV. Therefore, for $t\gtrsim3\times10^3$ sec, a significant part of the stopping power comes from nuclear interactions. In the Appendix we show that very-high-energy protons still lose their energy due to inverse Compton scattering and low-energy protons may have significant energy lost to plasma excitations, but protons which are marginally relativistic, or have energies less than about 50 MeV, lose energy due to nuclear interactions. Thus, nuclear stopping is relatively unimportant for $t<3\times10^3$ sec, but for $t>3\times10^3$ sec, one must consider reactions such as $pp\to pn\pi^+$ or $p^4\text{He}\to ppnd$, etc., in a complete treatment of the problem.

The stopping power for (anti)neutrons scattering with electrons or photons is suppressed by $\sim T^2/m_i^2$ relative to that for charged particles. Electron scattering is adequate to thermalize neutrons as long as $T\gtrsim0.1$ MeV. Unlike protons, neutrons do not stop efficiently via photon scattering; so, below $T\sim0.1$ MeV, (anti)neutrons do not scatter except off of free nucleons and nuclear material. This fact may have dramatic consequences at late times. After ^{4}He has formed ($t\sim300$ sec)$\sim\frac{1}{4}$ of all baryons are locked into ^{4}He, so some of the stopping power is due to n^4He collisions. For neutrons with $E\gtrsim50$ MeV, one may expect fission of ^{4}He nuclei because of these interactions, resulting in extra free neutrons. We have not carefully calculated this effect. For most of this paper, we assume neutrons from X decays reach kinetic equilibrium without inducing ^{4}He fission. Neglecting this effect, and fission of ^{4}He due to the absorption of antiparticles, we have underestimated the deuterium production

in the time range 10^3-10^4 sec, by perhaps as much as a factor of 4 (Ref. 26). We note that inelastic np collisions result in energy loss for the incident neutron but do not, on average, induce any $p \rightarrow n$ reactions.

The only particle that never stops via electromagnetic interactions is the K_L. Therefore, in evaluating the strong-interaction cross sections $\langle \sigma\beta \rangle$, we use kinetic equilibrium for all particles but K_L, which we assume are relativistic with their initial energy distribution determined by fragmentation.

We now turn to calculating $f^i_{NN'}$. Since we are interested in temperatures less than a few MeV, we need only consider processes that are exothermic, except for K_L's. For our purposes, the main feature of low-energy exothermic reactions is that $\sigma\beta$ is nearly independent of β. This makes the thermal averaging particularly simple, $\langle \sigma\beta \rangle \simeq \sigma\beta$ at threshold. Furthermore, at threshold there are only a few reactions to consider. In particular, we may drop K^+ from our discussion since the reaction $K^+ n \rightarrow K^0 p$ has $Q = 2.8$ MeV. We cannot ignore K^- because of the possibility of forming strange baryons, e.g., $K^- p \rightarrow \Lambda \pi^0$.

B. Cross sections

We collect in Table I numerical values for the cross sections entering into our evaluation of $\Gamma^i_{NN'}$ and Γ^i_A. Charged-pion interactions with nucleons are exothermic at threshold for the processes $\pi^- p \rightarrow n\pi^0, n\gamma$ and $\pi^+ n \rightarrow p\pi^0, p\gamma$. Using the results of Roper, Wright, and Feld[27] for hadronic charge-exchange interactions, together with[28]

$$P = \frac{\sigma(\pi^- p \rightarrow n\pi^0)}{\sigma(\pi^- p \rightarrow n\pi^+)} = 1.52 \ , \qquad R = \frac{\sigma(\gamma n \rightarrow p\pi^-)}{\sigma(\gamma p \rightarrow n\pi^+)} = 1.3 \ , \tag{3.6}$$

and assuming that $R \simeq \sigma(\pi^- p \rightarrow n\gamma)/\sigma(\pi^+ n \rightarrow p\gamma)$, we arrive at the first two rows in Table I.

The threshold cross sections for K^- are estimated from the coupled-channel analysis of Martin and Ross:[29]

$$\begin{aligned}
&\beta\sigma(K^- p \rightarrow \Sigma^- \pi^+) \simeq 21 \text{ mb} \ , \\
&\beta\sigma(K^- p \rightarrow \Sigma^+ \pi^-) \simeq 9 \text{ mb} \ , \\
&\beta\sigma(K^- p \rightarrow \Sigma^0 \pi^0) \simeq 11 \text{ mb} \ , \\
&\beta\sigma(K^- p \rightarrow \Lambda \pi^0) \simeq 4 \text{ mb} \ , \\
&\beta\sigma(K^- n \rightarrow \Sigma^- \pi^0) \simeq 20 \text{ mb} \ , \\
&\beta\sigma(K^- n \rightarrow \Sigma^0 \pi^-) \simeq 20 \text{ mb} \ , \\
&\beta\sigma(K^- n \rightarrow \Lambda \pi^-) \simeq 20 \text{ mb} \ .
\end{aligned} \tag{3.7}$$

The cross sections are typically larger than for the charged-pion case because the mass differences between the initial and final states in $K^- N$ interactions are larger than in $\pi^\pm N$ interactions. In deriving these cross sections, we have ignored a small velocity dependence due to the coupling of channels with different kinematics. Also, we have not yet included the overall Coulomb enhancement in the $K^- p$ channels. We deal with the Coulomb factor momentarily. The cross sections in Table I for K^- are determined by multiplying the results in Eq. (3.7) by the appropriate branching ratios for hyperon decays into n and p (Ref. 19).

The last meson on our list is K_L. Since they do not thermalize, we are interested in kaon energies on the order of a few GeV, typical of jet fragmentation. There is no convenient compilation of experimental data for K_L beams interacting with nucleons, so we have estimated $K_L N$ cross sections from $K^- p$, $K^- n$, and $K^+ p$ scattering in the few-GeV region.[30] We assume that K_L interacts half as K^0 and half as $\bar{K}^0$ and that K^0 scattering resembles K^+ because of the strange quark while $\bar{K}^0$ resembles K^- because of the antistrange quark. In doing this averaging we do not include elastic scattering. To get the charge-exchange cross section, we observe that typically there is a 10% diffractive part to any strong interaction, which retains some knowledge of the initial state and therefore set the $p \leftrightarrow n$ cross sections at slightly less than half the total absorptive cross section.

We next turn to the case of injected baryons. If the de-

TABLE I. Cross sections in mb for charge exchange and annihilation processes, parameters in the Coulomb corrections [Eqs. (3.8) and (3.9)] and fraction of the charged-particle multiplicity for pions, kaons, and baryon-antibaryon pairs. See text for references.

Particle i	$\langle \sigma\beta \rangle^i_{np}$	$\langle \sigma\beta \rangle^i_{pn}$	$\langle \sigma\beta \rangle^i_{nn}$	$\langle \sigma\beta \rangle^i_{pp}$	$\gamma T^{1/2}$	$n_i/\langle n_{\rm ch} \rangle$
π^+	1.7	0	0	0	0	0.4230
π^-	0	1.5	0	0	0.359	0.4230
K^-	26	31	34	14.5	0.585	0.0535
K_L	7	7	10	10	0	0.0535
$p\bar{p}$	28	0	0	37	0.704	0.0235
$n\bar{n}$	0	28	37	0	0	0.0235

caying particle carries no baryon number, then we expect equal numbers of protons and antiprotons and also of neutrons and antineutrons. We inject baryons in pairs and treat them as mesons. For example, a $(p\bar{p})$ "meson" interacts with a neutron with a cross section $\sigma(\bar{p}+n\rightarrow\cdots)$ and induces one $n\rightarrow p$ interaction. We denote the cross section by $\langle\sigma\beta\rangle_{n\bar{p}}^{p\bar{p}}$ for the process $(p\bar{p})+n\rightarrow p\cdots$, with the understanding that only the antibaryon interacts. The nucleon antinucleon cross sections are taken from Ref. 31, where $\bar{p}$D scattering was studied. We note that there is some uncertainty here as the $\bar{p}n$ cross section in deuterium need not be the same as for free neutrons, especially when the incident momenta are very low. We have also ignored charge-exchange reactions such as $n\bar{n}\leftrightarrow p\bar{p}$ which are much smaller than $N\bar{N}$ and $N\bar{N}'$ annihilations. After 100 sec, antineutrons do not thermalize, so using threshold cross sections is not justified. The antineutrons annihilate on the fly. However, by this time, the neutron abundance is very small, so exact values for the $N\bar{N}$ cross section are not important as the only available nucleon target is the proton. In truth, antibaryons may annihilate on ^{4}He as well as protons, but we have ignored this effect. Similar remarks hold for antiprotons after $\sim 3\times 10^3$ sec.

Up until now we have ignored Coulomb corrections to the cross sections. When there are two oppositely charged particles in the initial state, the reaction rate is enhanced by the square of the wave function at the origin:

$$C^2=\eta(1-e^{-\eta})^{-1},\quad \eta=\frac{2\pi\alpha Z_1 Z_2}{v}\ , \tag{3.8}$$

where v is the relative velocity and Z_1, Z_2 are the two charges. We average over thermal distributions to obtain $\bar{C}^2(\gamma)$, where $\gamma=2\pi\alpha Z_1 Z_2\sqrt{\mu/2T}$ with reduced mass μ. Although we have determined $\bar{C}^2(\gamma)$ numerically we give its large- and small-γ approximations:

$$\bar{C}^2(\gamma)\simeq 1+\frac{\gamma}{\sqrt{\pi}}+\frac{\gamma^2}{6}\cdots,\quad \gamma\ll 1$$

$$\simeq\gamma,\quad \gamma\gg 1\ . \tag{3.9}$$

These expressions for $\bar{C}^2(\gamma)$ are accurate to 20% if one makes the transition from small to large γ at $\gamma=2$. In Table I we give the value of $\gamma T^{1/2}$ for T in MeV. The resulting value of $\bar{C}^2$ is then used as a multiplicative factor in the relevant cross sections.

The decay rates $\Gamma_{\rm D}^i$ enter into the expression for $f_{NN'}^i$. We use the Particle Data Group values[19] for $\Gamma_{\rm D}^i=\tau_i^{-1}$, except for K_L which has a multiplicative factor to account for its decaying in flight: $\Gamma_D^{K_L}=(m_K/\bar{E})\tau_{K_L}^{-1}$, where our model of jet fragmentation, discussed below, is used to determine the average kaon energy $\bar{E}$.

These entries of Table I, together with the numerical values of the particle lifetimes (and factor for K_L), x_p, η, and s are sufficient to determine $f_{NN'}^i$ using Eq. (3.4).

C. Particle multiplicities

To complete our evaluation of $\mathcal{N}_{N\rightarrow N'}$, it remains to determine the average number of species i produced per X decay, P_{Xi}. Each X decay produces a number of jets equal to the number of quarks or gluons. Particle multiplicities within a jet should be nearly independent of how the jet originates, so we use hadronic multiplicities measured in e^+e^- annihilation experiments. To get P_{Xi} we take the average charged-particle multiplicities for a given jet, multiply by the number of jets $N_{\rm jet}$ and the branching ratio for X to decay hadronically B_h, and scale by the fraction of the average charge multiplicity carried by particle species i:

$$P_{Xi}\simeq\langle n_{\rm ch}\rangle N_{\rm jet}B_h n_i/\langle n_{\rm ch}\rangle\ . \tag{3.10}$$

The general form of the perturbative calculation of the leading double logarithms to the average jet charged-particle multiplicity[32] fits well the average charge multiplicity in e^+e^- experiments from $\sqrt{s}\simeq 2$–40 GeV. The low-energy data together with the combined DESY PETRA data are fit by[33]

$$\langle n_{\rm ch}\rangle=n_0+a\exp\{b[\ln(s/\Lambda^2)]^{1/2}\}\ , \tag{3.11}$$

where $n_0=2.0\pm 0.2$, $a=0.027\pm 0.01$, $b=1.9\pm 0.2$, and $\Lambda=0.3$ GeV. Since this is the result for two jets, we divide the total charged-particle multiplicity by two. Furthermore, for convenience, we write $\sqrt{s}/\Lambda=2E_{\rm jet}/\Lambda$. Our expression for the average charge multiplicity for one jet with energy $E_{\rm jet}$ is therefore

$$\langle n_{\rm ch}(E_{\rm jet})\rangle=1+(0.027/2)\times\exp\{1.9[2\ln(E_{\rm jet}/\times 0.15\ \text{GeV})]^{1/2}\}\ . \tag{3.12}$$

The energy of the jet depends on the final state of the X decay. If at the parton level, X decays into three particles, we assume that $E_{\rm jet}=M_X/3$, and that $N_{\rm jet}$ equals the number of quarks at the parton level (excluding spectators). The final components of P_{Xi} are the fractions of the average charge multiplicity carried by pions, kaons, and antibaryons. Using the time-projection-chamber (TPC) results[34] at PEP with $\sqrt{s}=29$ GeV, we show the fractions in the last column of Table I. We have assumed that the number of K_L's equals the number of K^-'s, and the number of $\bar{n}$'s equals that of $\bar{p}$'s. The fractions $n_i/\langle n_{\rm ch}\rangle$ are taken to be constants throughout the range of $E_{\rm jet}$ considered.

We note some features of the particle fractions. First, baryons are much less numerous than mesons so even though the mesons may have smaller efficiencies for $p\rightarrow n$ reactions they are still competitive at $T\sim 1$ MeV. Second, in many of the reactions we consider, pions appear in the final state (e.g., $K^-n\rightarrow\Lambda\pi^-$ with $\Lambda\rightarrow p\pi^-$); however, we include in $n_i/\langle n_{\rm ch}\rangle$ only the primary pions from X decays. As justification, we see that primary pions are ~ 10 times more numerous than kaons. Third,

the values in Table I include decays of short-lived particles. For example, $n_{p\bar{p}}/\langle n_{\rm ch}\rangle$ includes p's and $\bar{p}$'s from Λ and $\bar{\Lambda}$ decays. Similarly $n_{\pi^-}/\langle n_{\rm ch}\rangle$ includes π's produced by K_S decay but not any from K_L or K^- decay because the longer-lived mesons interact in the detector before they decay. Conveniently, detector design makes a distinction between short and long lived that is compatible with our needs in considering the early Universe. Fourth, leading particle effects are not correctly included in the values of $n_i/\langle n_{\rm ch}\rangle$ in Table I. In e^+e^- experiments, the quarks are produced proportional to the square of their charge, so u- or c-quark production is enhanced a factor of 4 times the d, s, or b production. On the other hand, in X decays the branching ratios into various modes depend on details of the model. For example, suppose X decays primarily into a bottom quark. Then that b quark will inevitably decay weakly into a c quark which in turn decays into an s quark creating a kaon. The net result may be an enhancement in K production.

The cross sections and multiplicities of Table I together with Eqs. (3.2)–(3.5) enable us to suitably modify the standard nucleosynthesis computer code to accommodate quasistable nonbaryonic X particles. It remains only to discuss how the equations change for baryonic X.

D. Baryonic X

Suppose that each X decay produces f_p protons and f_n neutrons. Then the baryon-to-entropy ratio changes according to

$$\dot{y}_B=(f_p+f_n)\Gamma_X y_X \ . \tag{3.13}$$

When X decays before the deuterium bottleneck breaks, the neutron-to-proton ratio is altered unless f_n/f_p is tuned to $f_n/f_p=x_n/x_p$. The change in the neutron fraction due to direct injection of baryons is given by

$$\dot{x}_n=\frac{\Gamma_X y_X}{y_B}(f_n x_p-f_p x_n) \ . \tag{3.14}$$

We note that if f_p or f_n is negative (corresponding to net *antibaryon* injection), we decrease y_B as per Eq. (3.13); however, the effect on x_n is not determined by what is injected but by annihilation cross sections. For example, if the annihilation cross sections were isospin independent, then $\dot{x}_n=\dot{x}_p=0$. We do not deal further with $f_p, f_n<0$.

Finally, besides modifying the baryon content of the Universe, X particles also change the energy density, pressure, and if charged, modify the electron chemical potential. When the X particles decay, they add energy and hence entropy to the radiation fluid. For the most part we expect these effects to be small. Anticipating the results of Sec. IV, $y_X/y_B\lesssim 10^{-1}$, thus for $m_X\sim 100$ GeV we expect $\rho_X/\rho_\gamma\approx 10^{-5}(1\ \text{MeV}/T)$. Nonetheless, we have included density, entropy generation, etc., in our numerical work and examined some peculiar cases where $\rho_X/\rho_\gamma\gtrsim 1$.

E. Summary

To summarize, our changes to the standard BBN rate equations are (1) to include the $n\leftrightarrow p$ conversions in the rate equations for the neutron and proton fraction of nucleons according to Eqs. (3.1) and (3.2), and for baryonic X, the terms dictated by Eqs. (3.13) and (3.14) and (2) to include the energy density of X particles and the entropy created by subsequent decay.

Our primary assumptions, which we have justified, are as follows.

(a) The injected hadrons are essentially stopped before they interact with ambient nucleons, so threshold cross sections are applicable.

(b) We may neglect the secondary production of hadrons, e.g., the pions from $K^-n\rightarrow\Lambda\pi^-\rightarrow p\pi^-\pi^-$.

(c) Photofission of light elements is unimportant before 10^4 sec.

(d) Neglecting ^{4}He fission induced by fast neutrons or antiparticles does not qualitatively modify our conclusions.

IV. RESULTS AND APPLICATIONS

A. Results

With fixed values of the standard BBN parameters τ_n and N_ν, our results depend on numerous parameters. We use the strong-interaction cross sections and particle multiplicities of Table I. The remaining parameters, defined in Sec. III, are y_X, m_X, B_h, $N_{\rm jet}$, $E_{\rm jet}$, f_p, f_n, τ_X, and the final value of the baryon to photon ratio η. It will sometimes be convenient to separate the baryon number due to X from the baryon number contained in protons and neutrons before X decays. We let η^0 denote the baryon to photon ratio of all baryons except X (or X decay products).

In the limit that $\rho_X\ll\rho_\gamma$ (which we assume for the moment), the mass dependence of our result appears indirectly through $E_{\rm jet}$. There are two places where $E_{\rm jet}$ enters: as mentioned in Sec. III, for K_L decays there is a boost factor $\gamma=E_{K_L}/m_K=E_{\rm jet}/[\langle n(E_{jet})\rangle m_K]$. This is a minor effect. The more influential dependence on m_X is through $\langle n(E_{\rm jet})\rangle$ directly, as it scales the total number of particles of each species i in the final state of X decays. We define F:

$$F=\frac{N_{\rm jet}B_h}{2}\frac{\langle n(E_{\rm jet})\rangle}{\langle n(33\ \text{GeV})\rangle} \ . \tag{4.1}$$

The value of F is unity when

$$\begin{aligned} &m_X=100\ \text{GeV}, \quad N_{\rm jet}B_h=2 \ , \\ &E_{\rm jet}=m_X/3\simeq 33\ \text{GeV} \ . \end{aligned} \tag{4.2}$$

Then, for nonbaryonic X, the two free parameters are τ_X and the initial value of $y_X F$, where the initial value is defined at the temperature $T=10^{11}$ K$=8.6$ MeV. The baryonic X decays have a more subtle scaling with m_X because the evolution equations have a dependence on $y_X f_p$ and $y_X f_n$ as well as on $y_X F$.

1. *Nonbaryonic X*

Be definition, X particles with zero baryon number require $f_n = f_p = 0$. We begin the presentation of our results with Fig. 2, where $\eta = 3 \times 10^{-10}$. We show separately the limits on $y_X F$ from considering only one of $\pi^{\pm}$, K^-, K_L, $p\bar{p}$, and $n\bar{n}$ injection, as well as the final result for injecting all six species. One should note that except for the $p\bar{p}$ injection, the hadronic species act to increase the ^{4}He abundance by converting more protons to neutrons than vice versa so our limit comes from requiring $Y \leq 0.26$. For $p\bar{p}$ injection, the effect goes the other way. The neutron-to-proton ratio is reduced by $p\bar{p} + n \rightarrow p \cdots$. The $p\bar{p}$ limits are derived from $Y \geq 0.22$. The net effect of all species together is always to increase the ^{4}He abundance.

At the shorter τ_X, it is a combination of all of the species that gives the bound on $y_X F$. The bounds are weakest there because of residual weak interactions, but at these lifetimes, mesons have their biggest effects because their interaction times are competitive with decay times. The baryon-antibaryon injection is the dominant factor for longer lifetimes. The shape of the limit curve in the regime $\tau_X \simeq 1-100$ sec is determined by two competing effects. As τ_X increases, the mesons become less important while baryon-antibaryon injection becomes more efficient as a source of neutrons. As x_n decreases due to neutron decay, the ratio of $p \rightarrow n$ to $n \rightarrow p$ reactions increases, resulting in more ^{4}He produced per X decay, and therefore a tighter limit on $y_X F$. For the case of $\eta = 3 \times 10^{-10}$, the meson effect is less important than the x_n effect and the limit improves with τ_X. However, for $\eta = 10^{-9}$ the mesons have a bigger initial effect and as a result the ^{4}He limit gets slightly worse as τ_X increases from ~ 3 to ~ 100 sec (see Fig. 4 below). After 100 sec, x_n drops to zero and only $n\bar{n}$ injection matters. The limit from ^{4}He has a slight upturn at $\tau_X = 10^4$ sec. At these late times, not all neutrons injected end up in ^{4}He because deuterium burning is not totally efficient. Also, we are approaching the time when neutrons decay before deuterium is formed.

Next we look at how the injection of hadrons affects the abundances of D, ^{3}He, and ^{7}Li. The limit on $y_X F$ from ^{4}He is approximately 10^{-12} over a wide range of lifetimes, so in Figs. 3(a)–3(c), we show with the solid line the light-element abundances as a function of τ_X for $y_X F = 10^{-12}$, $\eta = 3 \times 10^{-10}$, and $f_p = f_n = 0$. The factors controlling the ^{4}He curve have already been discussed. The D, ^{3}He, and ^{7}Li curves are unaffected by X decays until $\tau_X \simeq 100$ sec. For $\tau_X < 100$ sec, all the induced neutrons are eventually incorporated into ^{4}He. Very few decays occur late, when extra free neutrons affect the other nuclear abundances. For $\tau_X = 10^2 - 10^4$ sec, X_D increases, since for later times deuterium burning is less efficient, and so a larger residue of the extra neutrons remains in D. After 10^4 sec, the injected neutrons are likely to decay before they form D, so X_D drops. Very few neutrons from these late times find their way into ^{4}He. Having neglected photofission and baryon-induced fission on ^{4}He, the results for $\tau_X > 10^4$ sec in Fig. 3 illustrate only the effects of introducing thermal neutrons.

The ^{3}He abundance is linked to that of deuterium. For $\tau_X = 10^2 - 10^3$ sec, ^{3}He increases with the higher rate of DD burning, but after 10^4 sec, DD burning is not as efficient and $n\,^3\text{He} \rightarrow p\,\text{T}$ reactions decrease the amount of ^{3}He.

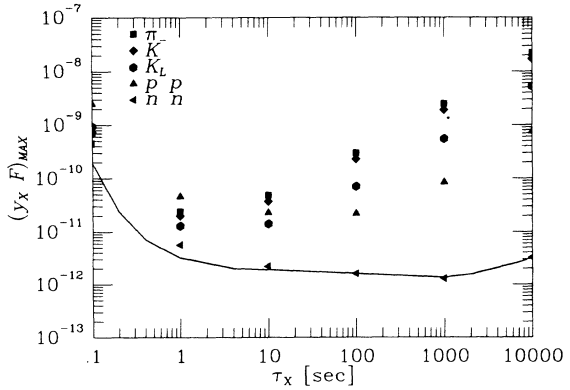

FIG. 2. Maximum values of $y_X F$ for $\eta = 3 \times 10^{-10}$ and $f_p = f_n = 0$. The limits from just $\pi^{\pm}$, K^-, K_L, $p\bar{p}$, or $n\bar{n}$ are shown separately.

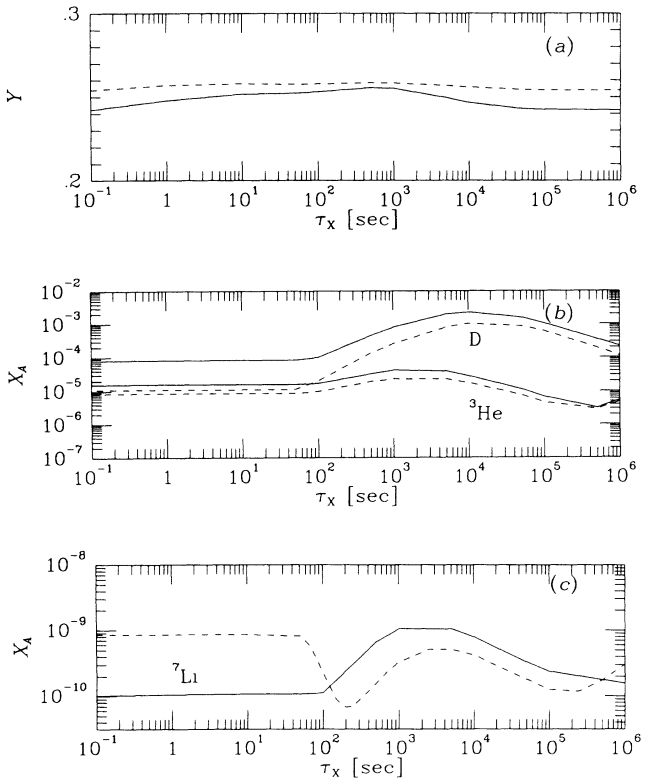

FIG. 3. ^{4}He, ^{3}He, D, and ^{7}Li abundances as a function of τ_X for y_X fixed at 10^{-12}, $\eta = (3, 10) \times 10^{-10}$, $f_p = f_n = 0$, and $F = 1$.

The effects for ^{4}He, D, and ^{3}He illustrated in Figs. 3(a) and 3(b) do not qualitatively depend on η as can be seen by comparing the solid lines ($\eta=3\times10^{-10}$) with the dashed lines ($\eta=10^{-9}$). The same cannot be said for ^{7}Li. For low η, we pointed out in Sec. II that ^{7}Li traces the tritium abundance, and therefore the deuterium abundance. We show this as the solid curve in Fig. 3(c) where $\eta=3\times10^{-10}$. For high η, the ^{7}Li comes predominantly from electron capture on ^{7}Be which happens very late. When there is an extra source of neutrons, the ^{7}Be may convert to ^{7}Li earlier via $n\,^7\mathrm{Be}\rightarrow p\,^7\mathrm{Li}$, which is then destroyed by $p\,^7\mathrm{Li}\rightarrow{}^4\mathrm{He}\,^4\mathrm{He}$. We can see this happening in the dashed curve of Fig. 3(c) for $\eta=10^{-9}$. As τ_X increases, the ^{7}Li curve drops as the ^{7}Be is eliminated, then grows again as direct production of ^{7}Li traces the D abundance.

From Figs. 3(a)–3(c), we see that for $\tau_X>100$ sec, D, ^{3}He, and ^{7}Li are much more sensitive than ^{4}He to injected hadrons. In fact, requiring $X_{\mathrm{D}}+X_{^3\mathrm{He}}\leq10^{-4}$ gives a much more stringent bound on y_XF than does ^{4}He. For $\eta=(3,10)\times10^{-10}$, the limits on y_XF from D plus ^{3}He and ^{4}He are shown in Fig. 4. The solid curve is the limit for $\eta=3\times10^{-10}$. The limits from D plus ^{3}He shown by the lower solid curve are more strict than necessary because even a marginal increase in $X_{\mathrm{D}}+X_{^3\mathrm{He}}$ violates the observational limit. The D+^{3}He curve for $\eta=10^{-9}$ in Fig. 4 at longer lifetimes is much less strict. Although the D and ^{3}He abundances increase, they now must increase an order of magnitude before the observational bound on $X_{\mathrm{D}}+X_{^3\mathrm{He}}$ is violated.

In the standard scenario, 10^{-9} is the upper limit on η from considering the deuterium abundance ($X_{\mathrm{D}}\geq10^{-5}$). With long-lived X particles, the deuterium abundance increases; therefore, we can consider larger values of η (Ref. 35), perhaps as large as 2×10^{-9} where $Y=0.26$ in the standard model. For example, if $\tau_X=10^3$ sec, $\eta=2\times10^{-9}$, and $y_XF=3\times10^{-14}$, then $Y\simeq0.260$, $X_{\mathrm{D}}\simeq1.8\times10^{-5}$, and $X_{^3\mathrm{He}}\simeq6.4\times10^{-6}$. As an added bonus, the ^{7}Li abundance is also acceptable, $X_{^7\mathrm{Li}}\simeq8.6\times10^{-11}$.

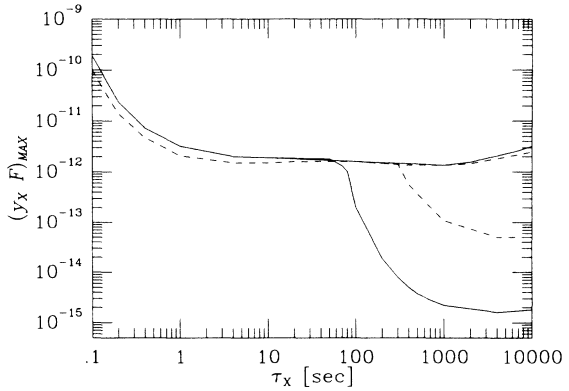

FIG. 4. Maximum values of y_XF for $\eta=3\times10^{-10}$ (solid line) and $\eta=10^{-9}$ (dashed line) with $f_p=f_n=0$. The limits come from both $Y\leq0.26$ and $X_{\mathrm{D}}+X_{^3\mathrm{He}}\leq10^{-4}$.

2. *Baryonic X*

The situation changes slightly when X carries baryon number: $f_p, f_n\neq0$. Precisely which unpaired baryon ultimately emerges depends on several effects, especially hadronization of the final-state parton. It is reasonable to set $f_p=f_n=0.5$, but we feel it is unreasonable to have $f_p\gg f_n$ or vice versa. Despite this prejudice, we consider several values of f_p and f_n. Otherwise, we keep the same parameter choices as in Eq. (4.2). Since baryon number changes as X decays we distinguish the baryon number originating in ambient protons and neutrons from that originating in X decays:

$$\eta=\eta^0+7.05(f_p+f_n)y_X\ , \tag{4.3}$$

where η^0 is the value of η if there were no X decay. In Fig. 5 we present limits on y_X for $\eta^0=10^{-9}$. The three curves (a) $f_n=0$, $f_p=1$ (dotted line), (b) $f_n=0.5$, $f_p=0.5$ (solid line), and (c) $f_n=1$, $f_p=0$ (dot-dashed line) arise from the limit $Y\leq0.26$. The lower branches to the solid curve represent the D+^{3}He limits for case (b) where they improve on the ^{4}He limit.

It is possible to understand the bounds in Fig. 5 by an appropriate rescaling of the $f_p=f_n=0$ results. The change in ^{4}He abundance due to a small amount of X decay may be written

$$\Delta Y=\frac{\Delta y_X}{y_B}[2\epsilon_4(a_n+f_n)-(f_p+f_n)Y]\ . \tag{4.4}$$

The (f_p+f_n) term is the dilution due to the increase in baryon number. The $2\epsilon_4(a_n+f_n)$ term reflects the increase in ^{4}He due to the direct injection of neutrons (f_n) and due to the production of neutrons via injected mesons and baryon-antibaryon pairs (a_n). The ϵ_4 parameter signifies that not every injected neutron ends up in ^{4}He, e.g., neutron decay, inefficient burning of deuterium, and induced $n\rightarrow p$ reactions may prevent neutrons from

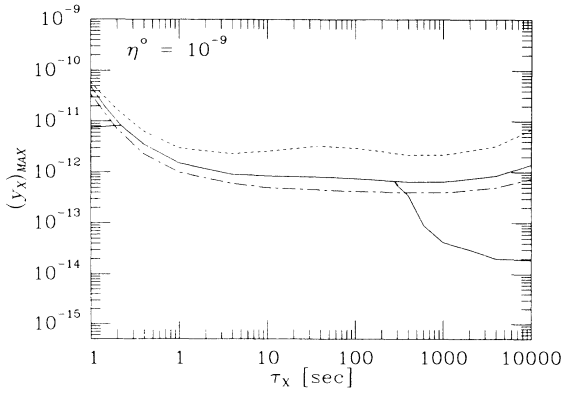

FIG. 5. Maximum values of y_X for $\eta^0=10^{-9}$, $m_X=100$ GeV, $N_{\mathrm{jet}}B=2$ and $f_p=1$, $f_n=0$ (dotted line), $f_p=f_n=0.5$ (solid line), and $f_p=0$, $f_n=1$ (dotted-dashed line), all coming from the limit $Y\leq0.26$. The lower branches of the solid line rely on $X_{\mathrm{D}}+X_{^3\mathrm{He}}\leq10^{-4}$.

being incorporated into ^{4}He. We can use Eq. (4.4) along with our limits for nonbaryonic X to predict a limit for $f_p, f_n \neq 0$:

$$(y_X)_{\max}(\tau_X, f_p, f_n) \simeq (y_X)_{\max}(\tau_X, 0, 0) \times \frac{2\epsilon_4 a_n}{2\epsilon_4(a_n+f_n)-(f_p+f_n)Y} . \quad (4.5)$$

The cleanest application of this relation is for $\tau_X \simeq 10^3$ sec, where a_n is the number of $n\bar{n}$ pairs per X decay and almost all neutrons are burned into ^{4}He, so $\epsilon_4 = 1$. For the parameter choice of Eq. (4.2), we find $a_n = 0.38$. Using our limit value, $Y = 0.26$, the ratios of $(y_X)_{\max}$ for the various values of (f_p, f_n) should be

$$(f_p=1, f_n=0) : (0.5, 0.5) : (0, 1) : (0, 0) :: 1.52 : 0.51 : 0.30 : 1.0 , \quad (4.6)$$

a result which is confirmed in Figs. 4 and 5. For larger τ_X, the scaling changes because ϵ_4 decreases (to ~ 0.5 at $\tau_X = 10^4$ sec). For small τ_X, ϵ_4 decreases slightly while the value of a_n increases because of meson interactions. There is one more effect; for $\tau_X < 1$ sec, the limits on y_X are so weak that a substantial increase in baryon number occurs. This results in an increase in ^{4}He just as in the standard nucleosynthesis scenario, so the $f_n + f_p = 1$ limits are all tighter at $\tau_X \lesssim 0.2$ sec than for the $f_n = f_p = 0$ case with the same η^0.

A similar rescaling can be done for the bounds derived from D plus ^{3}He for $\tau_X > 100$ sec. For simplicity let us ignore the ^{3}He. The deuterium abundance changes by

$$\Delta X_{\rm D} = \frac{\Delta y_X}{y_H}\{\epsilon_{\rm D}(a_n+f_n) - X_{\rm D}[f_p - (f_n+2a_n)(\epsilon_{\rm D}+\epsilon_4)]\} , \quad (4.7)$$

where $\epsilon_{\rm D}$ is the fraction of injected neutrons that end up in deuterium and $y_H = y_B(1-Y)$ is the density of hydrogen. Conveniently, whenever the deuterium constraint is important, $\epsilon_{\rm D} \gg X_{\rm D}$, and the values of $(y_X)_{\max}$ derived from D + ^{3}He are nearly proportional to $1/(a_n+f_n)$.

For lifetimes $\tau_X \lesssim 100$ sec the only effect of $f_p, f_n \neq 0$ is to change the value of η during the n and D burning phases. As seen in Fig. 3, extra neutrons injected early do not affect anything but ^{4}He, so the only constraint here is that y_X does not increase η so as to violate the usual nucleosynthesis constraints on deuterium. For $\eta^0 = 10^{-9}$ this limit is indicated by the lower branch of the solid line at $(y_X)_{\max} \simeq 8\times 10^{-12}$ below $\tau_X \simeq 0.3$ sec. Actually, this limit is artificially strong because $\eta = 10^{-9}$ is already marginal with respect to $X_{\rm D} \geq 10^{-5}$.

3. $\Omega_B = 1$

Many cosmological models suggest that $\Omega \equiv \rho/\rho_{\rm crit}$ should equal unity. The standard BBN model cannot accommodate a value of $\Omega_B = 1$. Too much ^{4}He is produced and not enough D. Nor is it possible to achieve $\Omega_B = 1$ in one of our models with $f_n = f_p = 0$, since ^{4}He always increases. It *is* possible, however, in a model with baryonic X. Before nucleosynthesis, part of the baryon number is contained in protons and neutrons, part in X. To get acceptable abundances of light elements, we must push parameters to the limits of being reasonable. For example, a Hubble constant $H = 50$ km/sec Mpc and $\eta = 7\times 10^{-9}$ gives $\Omega_B = 1$. Choosing $\tau_X = 10^3$ sec, $N_{\rm jet} B_h = 1$, $m_X = 3$ GeV (and $E_{\rm jet} = 1$ GeV), $f_p = 1$, $f_n = 0$, $\eta^0 = 6.3\times 10^{-9}$, and $y_X = 10^{-10}$, the light element abundances are $Y \simeq 0.250$, $X_{^3{\rm He}} \simeq 2.0\times 10^{-5}$, $X_{\rm D} \simeq 7.2\times 10^{-5}$, and $X_{^7{\rm Li}} \simeq 9.7\times 10^{-11}$. This is only one specific choice that gives acceptable values. The essential features are that f_p is near unity, f_n is near zero, and m_X is small so that there are few neutrons introduced, enough to increase D but not enough to increase ^{4}He which is decreased by the dilution term in Eq. (4.4).

4. Large ρ_X

Our analysis thus far has been based on η (or η^0) at times just before nucleosynthesis lying in the range allowed by the standard BBN model, then limiting values of y_X. One may argue that we are prejudicing our results to small values of y_X, and that a substantial departure from the standard BBN model is unconstrained. There are two types of extreme circumstances: for either baryonic or nonbaryonic X, the present value of η results from an earlier large baryon number "diluted" by entropy producing X decays.[7] The second possibility is for baryonic X only, where most of the present baryon number comes from the X decays themselves so $\eta \gg \eta^0$. We consider the two scenarios in turn.

Whether or not X carries baryon number, the case where the baryon number is diluted to a large degree by X decays does not work for m_X less than $\sim 10^7$ GeV if X decays hadronically. This is because only a few neutrons may be injected without seriously modifying the light-element abundances. From our results above we take the rather conservative limit $n_{n\bar{n}} < n_B$. The number of neutrons injected is $n_{n\bar{n}} = 0.0235\langle n_{\rm ch}\rangle N_{\rm jet} B_h n_X$. After the X's decay, the temperature is $T_X \sim \rho_X^{1/4}$, and $\eta \sim n_B/T_X^3$. Requiring $n_{n\bar{n}} < n_B$ is then equivalent to requiring

$$m_X \gtrsim \frac{0.0235\langle n_{\rm ch}\rangle}{\eta} N_{\rm jet} B_h T_X . \quad (4.8)$$

So, for $T_X \sim 0.1$ MeV, $\eta \sim 10^{-9}$, $N_{\rm jet} B_h = 1$, and taking into account the growth in multiplicity with m_X, we find $m_X \gtrsim 10^7$ GeV. An additional source of neutrons is from hadronic showers produced by high-energy photons associated with X decays. The threshold energy for photons to pair produce hadronic showers in collisions with background photons is roughly $E_h \sim (1\ \text{GeV})^2/T$, so even at $T = 10$ keV, photons with $E_h \sim 10^5$ GeV produce $N\bar{N}$ pairs. Since $E_h \sim 10^5$ GeV is less than the critical value of $m_X \sim 10^7$ GeV, we anticipate that no value of m_X is allowed. For $\tau_X < 0.1$ sec, the constraint gets much weaker as X decays well before nucleosynthesis. For $\tau_X > 10^4$ sec, the very large injection of photons (which must accompany a hadronic shower) causes considerable photofission and it seems unlikely that a large dilution factor is acceptable.[36]

We consider next the possibility that $n_B \ll n_X$ but $\rho_X \ll \rho_r$, so X carries essentially all of the baryon asymmetry, but there is little dilution. For $\tau_X < 0.1$ sec, this is certainly a viable alternative to the standard model because n/p is brought approximately to its equilibrium value by weak interactions. The problem with injecting later is that it is difficult to maintain the standard-model value for n/p. For $\tau_X \sim 0.1$–100 sec and for $\eta \leq 10^{-9}$, it is possible to find a satisfactory value for the ^{4}He, ^{3}He, and D abundances, but only for unlikely parameter values chosen to keep the $n\bar{n}$ injection rate low. As we suggested earlier, $f_p = f_n = 0.5$ are plausible values, while an acceptable range of Y in this scenario requires tuning f_p to be large and f_n to be small. For example, to minimize $n\bar{n}$ injection, take $m_X = 10$ GeV and $N_{\rm jet} B_h = 1$. For $\tau_X = 10^2$ sec and $y_X = 1.42 \times 10^{-10}$ ($\eta = 10^{-9}$), we find that $Y = 0.248$ and $X_{\rm D} + X_{^3{\rm He}} = 6.7 \times 10^{-5}$ for $f_p = 0.9$ and $f_n = 0.1$. For longer lifetimes, the problem is not so much the production of ^{4}He, rather the overproduction of D. By $\tau_X = 200$ sec, for the same value of y_X as in the example above, choosing $f_p = 0.927$ and $f_n = 0.073$ yields the minimum $Y = 0.220$, but $X_{\rm D} + X_{^3{\rm He}} = 1.4 \times 10^{-4}$.

For larger values of η, specifically $\eta = 7 \times 10^{-9}$, the question of consistency with the observed abundances is less straightforward. At short lifetimes, residual weak interactions and $n\bar{n}$ interactions make too many neutrons and overproduce ^{4}He, just as in the standard model. For $\tau_X = 10$–100 sec, acceptable values of Y are possible but with too little deuterium. Between lifetimes of a few hundred sec and almost 10^3 sec, for $f_p > 0.9$ and $f_n < 0.1$ with $f_p + f_n = 1$, we calculate that Y, $X_{\rm D}$, and $X_{^3{\rm He}}$ are all in acceptable ranges. By $\tau_X = 10^3$ sec, imposing $Y \geq 0.220$ implies $X_{\rm D} \geq 10^{-4}$. We conclude that it is possible to have $\Omega_B = 1$ with all baryons derived from X decays, for τ_X of a few hundred sec and f_p nearly equal to unity.

B. Applications

Our results are applicable to a wide variety of models. Unstable particles are likely to have decay modes with strongly interacting particles in the final state. We present limits on gravitinos, decaying photinos, and mirror quarks as examples of how our results may be used.

1. Gravitinos

Gravitinos in supergravity theories decay slowly via nonrenormalizable gravitational couplings, so they are natural candidates for the exotic X particle constrained here. Numerous analyses of the decay $\tilde{G} \to \gamma\tilde{\gamma}$ have appeared in the literature.[8,9,11] We consider instead the channel[11,12] $\tilde{G} \to g\tilde{g}$. A discussion of how our analysis differs from the recent work of Dominguez-Tenreiro[11] is described below.

Without inflation, the gravitino energy density may cause problems by either closing the Universe or contributing too much to the expansion rate of the Universe during the time of nucleosynthesis.[37] An appealing theory for many other reasons, inflationary universe models solve this problem by diluting the number of gravitinos; however, to account for the present value of η, the reheating temperature T_R must be higher than of order[38] 10^{10} GeV in conventional theories of baryogenesis. The relative abundance of gravitinos before nucleosynthesis is[39]

$$y_{\tilde{G}} = 3.34 \times 10^{-14} \left[\frac{T_R}{10^9\ \text{GeV}} \right] \times \left[1 - 0.018 \ln \left[\frac{T_R}{10^9\ \text{GeV}} \right] \right], \tag{4.9}$$

so the limit on T_R yields $y_{\tilde{G}} \gtrsim 3 \times 10^{-13}$.

The reheating temperature determines the abundance of gravitinos, and there is a fixed dependence of the lifetime on the mass. Consequently, our limits on $y_X F$ as a function of τ_X can be translated to a limit on T_R as a function of $m_{\tilde{G}}$. For a lifetime range of 10^{-1}–10^4 sec, using the relation[40] $\tau_{\tilde{G}} = 2\pi M_P^2/(9 m_{\tilde{G}}^3)$ (including the nine channels open for gluino and photino final states), the applicable mass range is 2×10^3–9×10^4 GeV. Using $F = \frac{8}{9} \langle n_{\rm ch}(E_{\rm jet}) \rangle / \langle n_{\rm ch}(33\ \text{GeV}) \rangle$, a straightforward rescaling of the results shown in Fig. 4 with $\eta = 10^{-9}$ yields $(y_{\tilde{G}})_{\rm max}$ between 10^{-14} and 5×10^{-12} as indicated by the bold line in Fig. 6. The limit $y_{\tilde{G}} \gtrsim 3 \times 10^{-13}$ may be satisfied only for a limited range of lifetimes, $\tau_{\tilde{G}} \lesssim 0.4$ sec ($m_{\tilde{G}} \gtrsim 5 \times 10^4$ GeV). At $\tau_{\tilde{G}} = 0.1$ sec, values of $T_R \lesssim 1.5 \times 10^{11}$ GeV are consistent with $(y_{\tilde{G}})_{\rm max}$, leaving only a very narrow window of allowed reheating temperatures for gravitino masses below 10^5 GeV.

Also shown by solid lines in Fig. 6 are limits on $y_{\tilde{G}}$ derived by Dominguez-Tenreiro[11] and Juszkiewicz, Silk, and Stebbins.[9,41] We note that the limit in Ref. 9 is from photodissociation of deuterium assuming $\tilde{G} \to \tilde{\gamma}\gamma$, while ours is from deuterium and ^{4}He creation assuming $\tilde{G} \to \tilde{g}g$. We have not included photodissociation in our calculations, but we see from Fig. 6 that it should be less important for $\tau_X < 10^4$ sec. In fact, this is to be expected since before 10^4 sec, photofission is suppressed because photons are absorbed by $\gamma\gamma$ pair production before they can cause photofission of D. Furthermore, any neutrons released by photofission may be recombined into D, as seen in Fig. 3.

The Dominguez-Tenreiro results are more directly

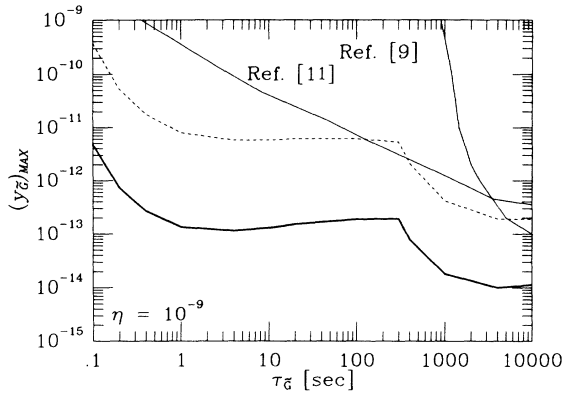

FIG. 6. Maximum gravitino abundance $y_{\tilde{G}}$ vs lifetime $\tau_{\tilde{G}}$. The bold line shows our result, and the other solid lines indicate the limits from Dominguez-Tenreiro (Ref. 11) and the photofission results of Juszkiewicz, Silk, and Stebbins (Ref. 9). The dotted line is a rescaling of our limits to compare with the Dominguez-Tenreiro limits. See text for details about the rescaling.

comparable because the gluino channel is included. A numerical comparison of our result (bold line) with the result of Ref. 11 shows a large discrepancy throughout the range of lifetimes; however, our analyses differ in several important ways.[42] The main difference in our conclusions arises from the treatment of particle multiplicities. In Ref. 11 the number of antinucleons per gravitino decay is fixed, independent of $m_{\tilde{G}}$, to be 0.2. For the range of masses between 2×10^3 and 9×10^4 GeV, the number of antinucleons per gravitino decay in our analysis ranges between 4 and 19. A rescaling of our result so that a constant 0.2 antinucleons are injected is shown by the dashed line in Fig. 6. Even with this rescaling, for $\tau_X\sim0.1-100$ sec, our limits differ by as much as a factor of 30. The discrepancy is partly accounted for by our inclusion of mesons (see Fig. 2), and the use of different parameters in the standard BBN model. We use $N_\nu=3$ and $Y\leq0.26$, instead of $N_\nu=2$ and $Y\leq0.25$. We are able to approximately reproduce the values of $(y_{\tilde{G}})_{\max}$ in Ref. 11 at $\tau_X=0.1$ and 100 sec by "turning off the mesons," fixing the nucleon-antinucleon injection number at 0.2, and using the values $Y\leq0.26$ and $N_\nu=2$. However, at $\tau_X=1-10$ sec our bound is still about a factor of 10 stronger. The difference cannot be accounted for by a slight difference in nucleon-antinucleon annihilation cross sections. We tried using isospin-independent cross sections as in Ref. 11 and our results changed by less than 15% (see Sec. VI). The last difference is that Dominguez-Tenreiro has included effects due to photodissociation and annihilation of $\bar{p},\bar{n}$ on ^{4}He. However, these mechanisms are inoperative for τ_X as short as 1–10 sec.

From a comparison of our results and those of Refs. 8, 11, and 17 a consistent picture of the importance of photofission in the lifetime range $10^4<\tau_X<10^6$ sec may be achieved. In Ref. 11, the effects of photofission of deuterium and D production induced by hadrons are comparable in the lifetime range of 10^4-10^6 sec. However, we believe their injection rate for $N\bar{N}$ pairs is too small by more than an order of magnitude. So, we conclude that photofission is not important for gravitino decay. This is borne out by comparing our results (bold curve) with that for Ref. 9 as shown in Fig. 6. Furthermore, this conclusion is in agreement with Dimopoules, Esmailzadeh, Hall, and Starkman[17] (DEHS). To achieve an acceptable deuterium abundance, DEHS must balance production and destruction, which requires $m_X/B_h\sim5\times10^4$ GeV. For the case in Fig. 6, at $\tau_{\tilde{G}}=10^4$ sec, we have $m_X/B_h=2\times10^3$ GeV (we assume a branching ratio to hadrons of $B_h=1$). Since the photodestruction scales linearly with m_X, for our parameter choice DEHS would overproduce deuterium. In other words, the constraint from overproduction is much stronger that the constraint from destruction of deuterium for gravitinos that decay to gluon-gluino.

This brings us to our last remark pertaining to gravitinos: what happens when the gluino channel is kinematically closed? Even then, there should be about a 1% branching ratio where the photon in the $\tilde{\gamma}\gamma$ channel is virtual and decays into a quark-antiquark pair. Even with a 1% branching ratio, rescaling our result in the regime $1<\tau_{\tilde{G}}<10^3$ sec yields a limit $(y_{\tilde{G}})_{\max}\lesssim10^{-11}$. By comparison, if the photinos resulting from gravitino decay have $m_{\tilde{\gamma}}=100$ GeV, then requiring their density to be less than closure density yields $(y_{\tilde{G}})_{\max}\lesssim10^{-11}$ as well,[9] and the limits based on the gravitino energy density during nucleosynthesis are weaker by 2–3 orders of magnitude. More interesting, perhaps, is to notice that now m_X/B_h is in the range required by DEHS to produce an acceptable abundance of deuterium.[17]

2. *Decaying photinos*

Conventional supersymmetric standard models conserve a reflection symmetry called $\tilde{R}$ parity, under which ordinary particles are even under reflection, and supersymmetric particles are odd under reflection. It can be shown that when baryon number and lepton number are conserved, the $\tilde{R}$-parity operator can be written as

$$\tilde{R}=(-1)^{2S+L+3B}, \tag{4.10}$$

where S, L, and B are spin, lepton number, and baryon number, respectively. When $\tilde{R}$ parity is a good symmetry, the lightest supersymmetric particle is stable. We shall assume here that the photino is the lightest supersymmetric particle.

Models with $\tilde{R}$-parity violation allow the photino to decay through B- or L-violating processes. Experimental constraints on explicit L- and B-violating terms in the Lagrangian[43] and scalar neutrino vacuum expectation values[44] have been studied in detail and shown to be unrestrictive on cosmological time scales. Cosmological bounds provide constraints on a new region of parameter space.[10]

To convert the results of Sec. IV A to the case of the photino, recall that the cosmological abundance of pho-

tinos is determined by the photino annihilation cross section. For t-channel scalar-fermion exchange in photino-photino annihilation into two fermions, the relative abundance of photinos at temperatures of ~ 10 MeV is[45]

$$y_{\tilde{\gamma}} \simeq 3.3\times 10^{-7}\left[\frac{m_{\tilde{f}}}{100\ \text{GeV}}\right]^4\left[\frac{1\ \text{GeV}}{m_{\tilde{\gamma}}}\right]^3 \tag{4.11}$$

for the common mass $m_{\tilde{f}}$ of scalar and pseudoscalar particles $\tilde{f}$ and massless fermions in the final state. Using Eq. (4.11), we can convert the maximum values of $y_X F$ in Fig. 4 into a mass versus lifetime plot for the photino. As an example, we suppose that $\tilde{\gamma}\to q\bar{q}\nu$ is the dominant decay mode at the parton level. Such a final state is allowed by a lepton-number-violating term[46] such as $C\psi_q\phi_{\bar{q}}\psi_\nu$. For this decay, $N_{\text{jet}}=2$ and we assume that $B_h=1$. The mass versus lifetime for a decaying photino is shown in Fig. 7. We have taken the maximum value of $y_X F$ for $\eta=(3,10)\times 10^{-10}$. By hypothesis, the photino is the lightest supersymmetric particle, so $m_{\tilde{\gamma}}<m_{\tilde{f}}$ for all lifetimes. Lifetimes beyond 2×10^3 sec for $m_{\tilde{f}}=50$ GeV, and beyond 2 sec for $m_{\tilde{f}}=250$ GeV are ruled out for the full range of photino masses. The limits of Fig. 7 can be transferred to limits on parameters in the Lagrangian. For example, if the term involving C is responsible for photino decay, we exclude a region of C vs $m_{\tilde{\gamma}}$ parameter space. Taking $m_{\tilde{f}}=250$ GeV and assuming $q=b$ in the final state, the exclusion of $\tau_{\tilde{\gamma}}>2$ sec is equivalent to requiring $C>8.2\times 10^{-8}(10\ \text{GeV}/m_{\tilde{\gamma}})^{5/2}$. Values of C such that $\tau_{\tilde{\gamma}}>10^4$ sec are ruled out by photofission of D or ^{4}He in Ref. 10. Similar limits apply for other possible decay mechanisms including those that violate baryon number.

Models with $\tilde{R}$-parity violation so small as to be applicable on cosmological time scales are natural in models with intermediate scales, for example, some low-energy superstring-inspired models. It has been proposed that small explicit $\tilde{R}$-parity violation may occur through higher dimension operators that conserve a discrete symmetry forbidding low-dimension $\tilde{R}$-parity-violating operators.[13] Depending on the dimension of the operator and the scale of $\tilde{R}$-parity breaking, the photino lifetime ranges from very short to the age of the Universe. With our results, we are in principle able to constrain the scale of $\tilde{R}$-parity violation as a function of d, the dimension of the operator by which $\tilde{R}$ parity is violated. In practice, counting decay modes and including all of the coupling constants properly is very model dependent. To give a sense of the types of bounds that one may find, consider the induced dimension-six operators of Ref. 13 that yield a decay time

$$\tau_{\tilde{\gamma}} \sim 10^{-18}\left[\frac{M}{10^4\ \text{GeV}}\right]^4\left[\frac{100\ \text{GeV}}{m_{\tilde{\gamma}}}\right]^5 \text{sec}\ . \tag{4.12}$$

By requiring $\tau_{\tilde{\gamma}}\lesssim 2$ sec, the limit on the intermediate scale M where $\tilde{R}$ parity is broken is $M\lesssim 3.8\times 10^8$ GeV$(m_{\tilde{\gamma}}/100\ \text{GeV})^{5/4}$ for $m_{\tilde{f}}=250$ GeV. Even with $\tau_{\tilde{\gamma}}\lesssim 2\times 10^3$ sec, the limit on M, $M\lesssim 2\times 10^9$ GeV$(m_{\tilde{\gamma}}/100\ \text{GeV})^{5/4}$, is lower than typical values, $M\sim 10^{10}$–10^{14} GeV (Ref. 47), which are required in realistic models predicting the weak mixing angle.

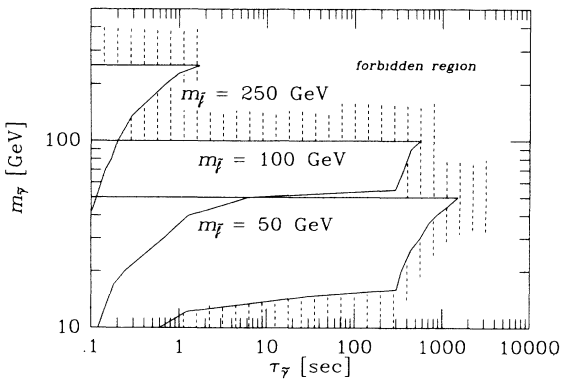

FIG. 7. Mass vs lifetime for a decaying photino when $m_{\tilde{f}}=50$, 100, 250 GeV.

3. *Mirror quarks*

Mirror quarks in certain grand unified theories have lifetimes on the order of seconds. A mirror-quark family contains charge $\pm\frac{1}{3}$, $\pm\frac{2}{3}$ fermions with the same $SU(2)_W$ content as ordinary quarks, except with chiralities interchanged. The essential feature is that mirror-quark electroweak representations permit a bare mass term between an ordinary quark doublet and a mirror-quark doublet.

In the O(18) family unified model,[14] there are equal numbers of ordinary and mirror families, so in the absence of additional symmetries, all ordinary fermions gain large bare masses. A mirror parity is introduced under which ordinary quarks are even, and mirror quarks are odd. This forbids bare masses; however, a strictly conserved mirror parity introduces a new problem. The lightest mirror quark is a stable strongly interacting particle with a weak scale mass. Limits on the presence of heavy strongly interacting particles in water[48] and in iron[49] effectively exclude the possibility. The solution to this problem is to ensure that mirror quarks decay to ordinary quarks through higher dimension operators. In a model without an intermediate scale, the only possibilities are dimension-five operators. In terms of the unification scale M_{GUT} and the mass of the mirror quark m_Q, the order of magnitude of the lifetime is $\tau_Q=(M_{\text{GUT}}/10^{15}\ \text{GeV})^2/(m_Q/10^2\ \text{GeV})^3$ sec.

The relative abundance of mirror quarks y_Q at the time of nucleosynthesis is not a number that has been calculated. In the absence of a mirror-quark asymmetry, $y_Q/y_q\simeq 10^{-10}$. This is well below the level of constraints imposed by our analysis. Realistically, a mirror-quark asymmetry is expected. Recall that the ordinary quark asymmetry arises through baryon-nonconserving interactions, violations of C and CP, and a departure from

thermal equilibrium.[50] All of these ingredients are expected to be present in the mirror-quark sector as well. Standard calculations of the baryon asymmetry in grand unified models depend on the imaginary part of products of Yukawa couplings. Since mirror quarks are heavier than ordinary quarks (else we would have seen them), it is plausible to assume that $y_Q \gtrsim y_q$, so that almost all baryons result from X decay. Taking $m_Q = 100$ GeV, $f_n = f_p = 0.5$, and $\eta^0 = 0$, we find that $\tau_Q \lesssim 0.1$ sec.

V. COLD-DARK-MATTER ANNIHILATION

In this section we consider the effects of hadronic particles that result from the annihilation of weakly interacting massive particles (WIMP's). We use the terminology WIMP's to distinguish them from other types of cold dark matter. There are a variety of astrophysical, cosmological, and particle-physics arguments that lead us to believe that WIMP's are likely to be an important constituent of our Universe.[3,15,21,45] At first thought, WIMP annihilation would not seem to be important at nucleosynthesis since annihilations for heavy particles freeze-out far above temperatures ~ 1 MeV. However, a small amount of annihilation still takes place, not enough to alter the abundance of WIMP's but still enough to affect nucleosynthesis. Therefore we present the annihilation rate. By multiplying this by the branching ratio to quarks to get jets of hadrons, the WIMP annihilation contribution to nucleosynthesis is introduced into our computer code. We examine its effects on light-element abundances.

The rate equation for the WIMP abundance[21] in terms of $y \equiv n_W / s$ is

$$\frac{dy}{dt} = -\langle \sigma\beta \rangle s (y^2 - y_{\rm eq}^2) , \tag{5.1}$$

where $y_{\rm eq}$ is the WIMP abundance if they were in thermal equilibrium, $\langle \sigma v \rangle$ is the thermal-averaged annihilation cross section, and s is the entropy. By the time of nucleosynthesis, y is essentially its final value y_∞, and the production term $\sim y_{\rm eq}^2$ is totally negligible. The rate equation at this time is approximately

$$\frac{dy}{dt} \simeq -\langle \sigma\beta \rangle s y_\infty^2 . \tag{5.2}$$

The final abundance of WIMP's is determined by the annihilation cross section at the time the production term becomes unimportant, which we shall denote by the subscript F, for "freeze-out":

$$\langle \sigma\beta \rangle_F y_\infty \simeq \frac{2\pi}{b^3} \frac{g_{\rho F}^{1/2}}{g_{sF}} \frac{(N+1)}{A_N} \frac{x_F^{N+1}}{m_W M_{\rm Pl}} , \tag{5.3}$$

where m_W is the WIMP mass, $M_{\rm Pl} = 1.22 \times 10^{19}$ GeV, and we define b by $s \equiv b^3 T^3$, g_ρ by $\rho \equiv \pi^2 g_\rho T^4/30$, and g_s by $b^3 \equiv 2\pi^2 g_s/45$. The N in Eq. (5.3) refers to a possible temperature dependence of the annihilation cross section near freeze-out, $\langle \sigma\beta \rangle \sim T^N$. For many candidate WIMP's, $N = 0$, i.e., the annihilation cross section is constant, while for others, $N = 1$. A transition between 0 and 1 is also possible. We take $N = 0$ as a typical value. The constant A_N has a value of $A_N = 1.0 \pm 0.2$ which depends mainly upon when freeze-out occurs with respect to the quark-hadron phase transition.[51] Lastly, x_F is defined by $x_F \equiv m_W / T_F$. For any model of interest, $x_F \simeq 20$, with only a logarithmic dependence on m_W, $\langle \sigma\beta \rangle$, etc. Since we are interested primarily in the range of masses $m_W \sim 5$–10 GeV, this fixes $T_F \sim 250$–500 MeV and, in turn, $b^3 \sim 27$. All told, this gives

$$\langle \sigma\beta \rangle y_\infty \simeq \frac{10}{m_W M_{\rm Pl}} \frac{\langle \sigma\beta \rangle}{\langle \sigma\beta \rangle_F} . \tag{5.4}$$

The ratio $\langle \sigma\beta \rangle / \langle \sigma\beta \rangle_F$ is less than or equal to one during nucleosynthesis. Finally, we observe that the abundance of WIMP's is related to their contribution to the density of the Universe by

$$y_\infty = 1.9 \times 10^{-9} h^2 \Omega_W \frac{1 \text{ GeV}}{m_W} , \tag{5.5}$$

where h is the Hubble constant in units of 100 km/sec Mpc and $\Omega_W \equiv \rho_W / \rho_{\rm crit}$ is the fraction of critical density supplied by WIMP's. For the purpose of scaling our results, we take $\Omega_W h^2 = \frac{1}{4}$. We then combine Eqs. (5.2), (5.4), and (5.5) to give

$$\frac{dy}{dt} = -7.2 \times 10^{15} \left[\frac{\Omega_W h^2}{0.25} \right] \frac{\langle \sigma\beta \rangle}{\langle \sigma\beta \rangle_F} \frac{s}{m_W^2 M_{\rm Pl}} \text{ sec}^{-1} . \tag{5.6}$$

This general expression is useful for a wide variety of cold-dark-matter models.

Before calculating numerically with Eq. (5.6) we make some estimates of what we expect. It is convenient for our estimate to give the annihilation rate in terms of the variable $x = m_W / T$:

$$\frac{dy}{dx} = -\frac{C y^2}{x^2} , \tag{5.7}$$

where $C \equiv [b^3 g_s / (2\pi g_\rho)]^{1/2} \langle \sigma\beta \rangle m_W M_{\rm Pl}$. With the same approximations as before concerning x_F, A, N, etc., we find that the change in y_W due to annihilation between temperatures T_1 and T_2 is

$$\Delta y_W = 8 \left[\frac{T_1 - T_2}{m_W} \right] y_\infty . \tag{5.8}$$

Expressing y_∞ in terms of the baryon abundance, $y_\infty = (\Omega_W m_B / \Omega_B m_W) y_B$, we find that the number of annihilations per baryon is

$$\frac{\Delta y_W}{y_B} \simeq 8 \frac{T_1 - T_2}{m_W^2} m_B \frac{\Omega_W}{\Omega_B} . \tag{5.9}$$

For illustrative purposes, we take $\Omega_W / \Omega_B = 10$ and $m_W = 5$ GeV. At the time the neutron-proton ratio is being fixed, $T \sim 0.5$ MeV. Taking $T_1 - T_2 \sim T_1$, the temperature at nucleosynthesis, we find $\Delta y_W / y_B \simeq 1.6 \times 10^{-3}$. In Sec. IV we found that in order for decaying particles to influence the neutron-proton ratio, we needed $y_X / y_B \gtrsim 10^{-1}$, so we do not expect WIMP annihilation to

greatly affect the helium abundance. The effects on the deuterium abundance are more dramatic simply because X_D is so small. At $T \sim 0.03$ MeV, $\Delta y_W / y_D \simeq 1$ for $X_D \simeq 10^{-4}$. If there is a yield of one neutron per WIMP annihilation, the deuterium abundance may be increased dramatically.

With this motivation, we use the annihilation rate of Eq. (5.6) as the injection mechanism for hadronic matter in our modified nucleosynthesis code. We assume that annihilation proceeds via $WW \to q\bar{q}$ with a branching ratio B_q. The $q\bar{q}$ pair produces two jets, each of energy $E_{\rm jet} = m_W$, which are fragmented according to the algorithm in Sec. III. We study a model where $\eta = 4 \times 10^{-10}$ and $m_W = 5$ GeV. The light-element abundances are shown in Fig. 8 as a function of the injection parameter I:

$$I = B_q \left[\frac{\Omega_W h^2}{0.25} \right] \frac{\langle \sigma\beta \rangle}{\langle \sigma\beta \rangle_F} \frac{\langle n_{\rm ch}(m_W) \rangle}{\langle n_{\rm ch}(5\ {\rm GeV}) \rangle} \frac{25\ {\rm GeV}^2}{m_W^2} . \tag{5.10}$$

The particle multiplicity $\langle n_{\rm ch}(E_{\rm jet}) \rangle$ is given in Eq. (3.12). As one can see in Fig. 8, the observed limits on light-element abundances are transcended at $I \simeq 23$ (^{4}He), $I \simeq 5.5$ (D+^{3}He). At an intermediate value, $I \simeq 15$, the ^{7}Li bound is violated.

Naively, $I \lesssim 1$, however there are several reasons why I may be larger. By slightly reducing m_W, I increases; for example, the mass of a Dirac neutrino that provides $\Omega h^2 = \frac{1}{4}$ is between 3 and 4 GeV (Refs. 51 and 52). Un-

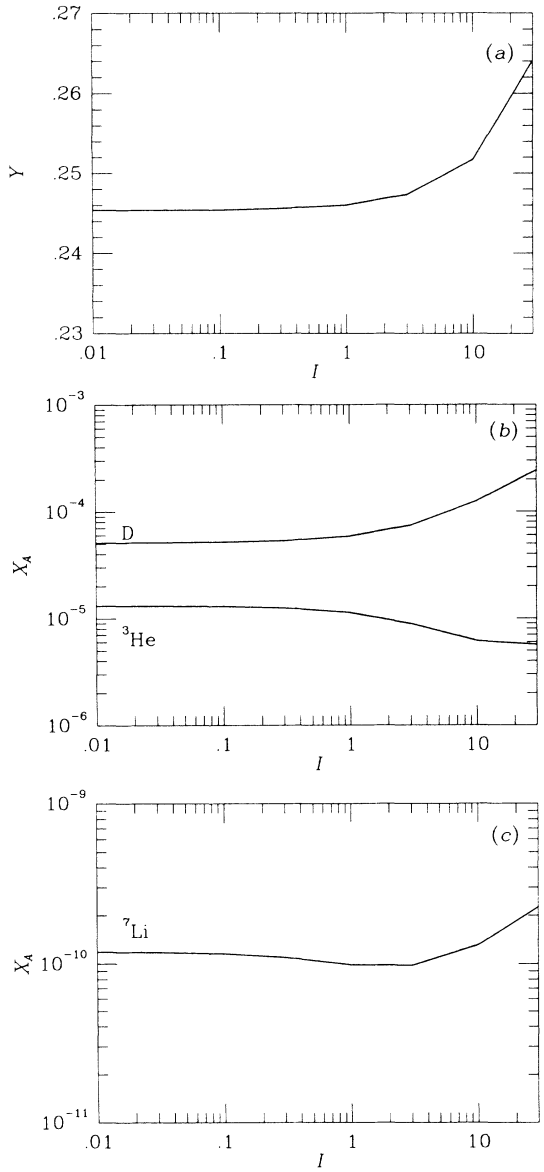

FIG. 8. The light-element abundances as a function of the injection parameter I for cold dark matter. Here $\eta = 4 \times 10^{-10}$ and $m_W = 5$ GeV.

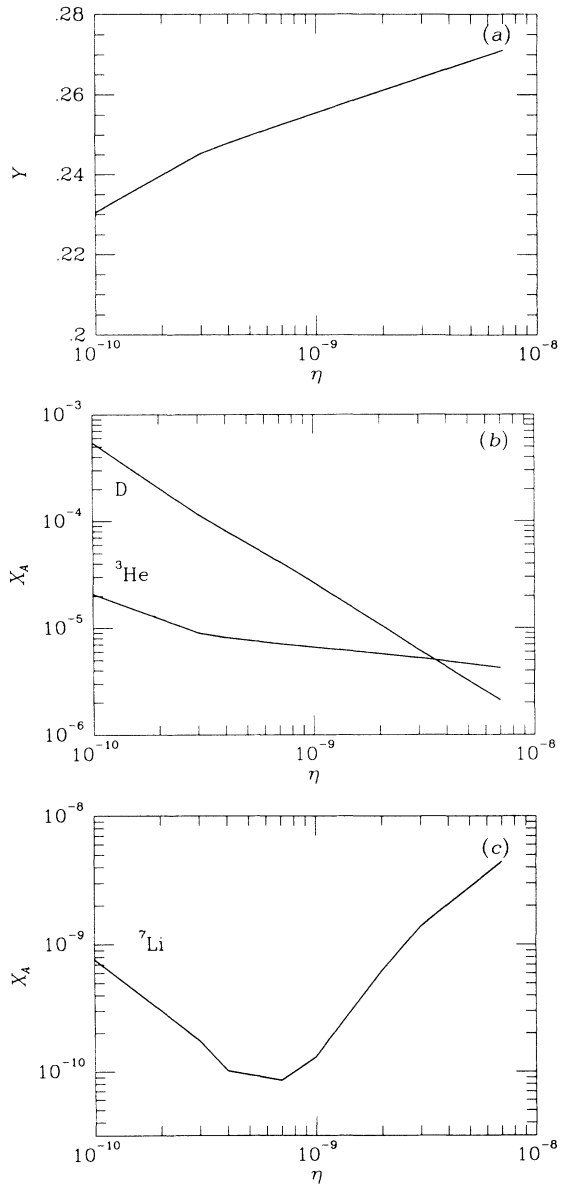

FIG. 9. The light-element abundances as a function of η for fixed $I = 4$ and $m_W = 5$ GeV.

certainties in determining the value of the Hubble constant[53] may amount to a factor of 2 in I. Finally, our calculations have been done without accounting for free neutrons produced from neutron dissociation and antibaryon absorption on ^{4}He. A compensation for the normalization of the number of free neutrons is to increase the *effective* value of I, perhaps as much as a factor of 2–4 at times relevant for determining the abundance of deuterium. Because of the uncertainty in the true value of I, we have forborne any attempt to constrain various combinations of nucleosynthesis and WIMP dark-matter parameters at this point.

In addition to constraining models, it is possible that previously ruled out values of η are now acceptable. Specifically, the strongest constraints on high-η models come from an underproduction of D and an overproduction of ^{7}Li through ^{7}Be. Both these problems are alleviated by the late injection of neutrons. To exhibit this effect, we show in Fig. 9 the light-element abundances for $I=4$ as a function of η. The constraints on η are relaxed. Now $\eta<1.8\times10^{-9}$ (^{4}He) and $\eta<2.1\times10^{-9}$ (D). From ^{7}Li, $\eta<1.1\times10^{-9}$. These results are for only one value of I. Clearly, it is possible for slightly higher I that the strongest constraint on η arises from the ^{4}He abundance. If this happens, Ω_B as high as 0.3 is not ruled out if the neutron half-life is taken to be 10.2 min (1σ lower than the mean value) or the number of massless neutrinos is two.[54] We do not advocate this approach as it seems to require believing several unlikely things; however, it would have interesting ramifications for a theory of galaxy formation in which a mixture[55] of baryons and cold dark matter is invoked to explain observations of peculiar velocities, large-scale structure (voids, etc.), and clustering of clusters of galaxies.

VI. DISCUSSION

We have presented general constraints on the relative abundance of X particles that decay into hadrons, based upon the effects those hadrons have on the abundance of light elements produced in primordial nucleosynthesis. Our conclusion is that for the lifetimes considered here, $\tau_X=0.1-10^4$ sec, the upper bounds on y_X are nontrivial; $(y_X)_{\max}\sim10^{-10}-10^{-14}$ for $m_X=100$ GeV. Turning the situation around, we have asked if hadronic decays of X particles may allow for a wider variation in the baryon-to-photon ratio than results from standard BBN. The answer is that $\eta<3\times10^{-10}$ is still prohibited, but $\eta>10^{-9}$ may be allowed since neutrons released from X decay may provide an additional source of deuterium and suppress the ^{7}Li abundance. However, to allow for $\Omega_B=1$ requires a fairly unnatural choice of parameters. In addition to studying decays, we conclude that annihilation of weakly interacting $\sim$5-GeV mass particles around 10^3 sec may significantly raise the upper limits on Ω_B derived from nucleosynthesis arguments.

The limits rely on a variety of parameters, all with uncertainties. The most obvious uncertainties are those associated with nucleosynthesis itself: the nuclear-reaction rates, N_ν, $\tau_{1/2}$ and η, as well as the numerical evaluation. The nuclear-reaction rates come from a combination of experimental and theoretical cross sections. Our version of the Wagoner computer program does not include the small corrections outlined by Dicus *et al.*[56] These corrections amount to a ~0.0025 decrease in Y, and 1–2% changes in the abundances for other light elements. The effect of decreasing N_ν by one in the standard model is to decrease Y by ~0.013 and decreasing $\tau_{1/2}$ by 0.1 min decreases Y by ~0.0014 (Ref. 57). Either of these two changes increases y_X approximately according to Eq. (4.4). Finally, the limits on the primordial abundances in Eqs. (2.1a)–(2.1d) have uncertainties associated with both the extrapolation of present observations to primordial limits, and with the measurements themselves.

The sensitivity of our results to the hadron-nucleon interaction cross sections depends on whether the hadron is a nucleon or meson. We have shown in Sec. IV that the neutron-antineutron pair injection and unpaired baryons are the most important effects for all but the shortest lifetimes. The entries in Table I are inferred from antiproton-deuterium scattering cross sections. We have compared our results using these values with those setting $\langle\sigma\beta\rangle=1$ mb, independent of isospin. The difference in limits from the $(n\bar{n})$ injection alone is less than 15% at short times, and by $\tau_X\simeq100$ sec, the results are identical. This is not surprising since there are so few neutrons after $t\sim100$ sec that antibaryons always react with protons, regardless of the cross section [see Eqs. (3.4) and (3.5)]. The absolute cross sections for meson-nucleon interactions are important for $\tau_X\lesssim10$ sec because of the competition between reactions and meson decays. Low-energy measurements of the charged meson-nucleon cross sections make our extrapolations to threshold fairly good. The absence of experimental data on low-energy K_L scattering makes our K_L cross sections less reliable; however, K_L's cause at most half the increase in ^{4}He for $\tau_X\lesssim10$ sec.

For the multiplicities, we have used PETRA values for $\langle n_{\rm ch}\rangle$ as a function of energy. The error in b in Eq. (3.11) can give a factor of 2 in $\langle n_{\rm ch}\rangle$ for $E_{\rm jet}=33.3$ GeV, and a factor of 3 for $E_{\rm jet}=10^5$ GeV. The value suggested by QCD, $b=1.77$, is intermediate between the central experimental value and the 1σ lower value. The uncertainty in a in Eq. (3.11) should be correlated with that in b to maintain the correct charged-particle multiplicity at low energies. We fix $\langle n_{\rm ch}\rangle$ for $\sqrt{s}=30$ GeV at the value obtained by using the central values of $a=0.027$ and $b=1.9$. Then, putting $b=1.7$, $a=0.05$ reproduces $\langle n_{\rm ch}\rangle$ for $\sqrt{s}=30$ GeV and differs only by a factor of 1.5 for $E_{\rm jet}=10^5$ GeV. In any case, more precise values can be incorporated by rescaling F. The same is true for the $n\bar{n}$ multiplicity when $n\bar{n}$ effects are dominant. We have used the TPC experimental value for $n_{n\bar{n}}/\langle n_{\rm ch}\rangle$ which is $\sim20\%$ lower than the PETRA value.[33] The TPC quoted errors on n_i at $\sqrt{s}=29$ GeV are $\sim10\%$. We do not expect the fractional multiplicities to be accurate for jet energies less than 5 GeV.

Throughout our analysis, we have left out three potentially important physical effects: photofission, neutron-induced fission, and absorption of antiparticles by ^{4}He. We expect photofission to be important only after 10^4 sec.

Indeed, from our discussion of the gravitino case, we expect photofission of deuterium to be less important than deuterium production for X particle masses less than about 10^4 GeV. Only for $\tau_X \gtrsim 10^6$ sec, when photofission of ^{4}He turns on, is photofission the dominant process. Again, an overabundance of D will result. These conclusions are not in conflict with DEHS where $m_X/B_h \sim 5\times 10^4$ GeV is required to achieve a proper deuterium abundance. The net effect of ^{4}He fission is to deplete the ^{4}He abundance and make either D, ^{3}He, or free nucleons. Before 10^3 sec, most of these can be reprocessed back into ^{4}He. Later, ^{4}He formation is not so efficient; however, D formation is, as may be seen in Fig. 3. For lifetimes longer than a few hundred seconds, overproduction of D yields the strongest bounds, so by including dissociation of ^{4}He, our limits would be strengthened.

For the case of baryonic X, we have made an implicit assumption that nuclear interactions of X particles are unimportant. For example, we might have worried about the possibility of forming (X^4He) bound states, but we did not. Baryonic X models may be divided into two classes: those with nuclear interactions and those without. An example of the first class would be mirror quarks, where the heavy quark is bound into a heavy baryon that has nuclear interactions at low energies. An example of the second class would be a photino which undergoes baryon-number-violating decays. Strictly speaking, our results only apply to the second class of models. However, one expects qualitatively similar results for the first class: extra neutrons tend to enrich the Universe with light elements.

ACKNOWLEDGMENTS

We thank P. Arnold, E. Kolb, Y. Meurice, M. Soldate, G. Steigman, and M. Turner for comments and discussions. We especially thank L. Kawano for providing us with his version of R. Wagoner's nucleosynthesis computer code. We thank the CERN Theory Division for their support and hospitality when this work was begun.

APPENDIX: ELECTROMAGNETIC STOPPING OF HADRONS

The purpose of this appendix is to present calculations of the stopping rate of hadrons due to scattering of electrons and photons. We are primarily interested in knowing when hadrons produced in jets thermalize electromagnetically before they interact strongly. The hadrons are relativistic when produced, so we estimate the time to lose their relativistic energy. Also, the temperatures of interest are much less than the mass of the hadrons, so we must also estimate the time to lose their nonrelativistic energy. Our analysis applies to both charged particles and neutrals with a magnetic dipole moment. Because of the large number of processes and the range of physical regimes, we have tried to take a unified approach to the problem. To this end, we have concentrated on the energy lost due to two-body scattering which is usually the dominant term. We have not included energy lost to collective excitations of the plasma.

The rate of energy loss due to elastic scattering with particles in the medium is

$$\frac{dE}{dt}=\sum_j \frac{g_j}{(2\pi)^3}\int n_j(\mathbf{k})[1\mp n_{jf}(\mathbf{k}_f)]\Delta\mathcal{E}_j\frac{d\sigma_j}{d\Omega}\times v_{\rm rel}\,d\Omega\,d^3\mathbf{k}\ , \tag{A1}$$

where the sum is over particle species j in the medium, g_j is the number of spin degrees of freedom for particle j, and the initial and final occupation numbers are $n(\mathbf{k})=(e^{\mathcal{E}/T}\pm 1)^{-1}$ for $\mathcal{E}$ the energy of particle. The upper signs refer to fermions, the lower to bosons. The relativistic generalization of the relative velocity of incident and target particles is $v_{\rm rel}=[(\boldsymbol{\beta}-\boldsymbol{\beta}_j)^2-(\boldsymbol{\beta}\times\boldsymbol{\beta}_j)^2]^{1/2}$ where $\boldsymbol{\beta}$ is the velocity of the incident particle and $\boldsymbol{\beta}_j$ is the velocity of the target. The center-of-mass cross section between incident and target particle is $d\sigma_j/d\Omega$.

The energy transfer in a collision is given by $\Delta\mathcal{E}_j=\mathcal{E}_{jf}-\mathcal{E}_j$. It depends on the incoming particle energy E and mass M, the target particle momentum $\mathbf{k}$ and mass m_j, and the center-of-mass scattering angles θ and ϕ through the relation

$$\begin{aligned}\mathcal{E}_{jf}=\mathcal{E}_j\gamma^2\gamma'(1-\beta\beta_j\cos\alpha)&\\ \times\{\gamma'[(1-\beta'\beta_2)(1-\beta\beta'\cos\psi)&\\ +(\beta'-\beta_2)(\beta\cos\psi-\beta')\cos\theta]&\\ -\beta(\beta'-\beta_2)\sin\theta\cos\phi\sin\psi\}\ .&\end{aligned} \tag{A2}$$

Equation (A2) is derived by taking the initial particles with velocities $\boldsymbol{\beta},\boldsymbol{\beta}_j$ and the definition $\cos\alpha\equiv\boldsymbol{\beta}\cdot\boldsymbol{\beta}_j$, performing a Lorentz transform Λ to the center-of-mass frame, scattering by angles θ,ϕ and then transforming by Λ^{-1} back to the rest frame of the medium. The Lorentz transformation may be broken up as $\Lambda=\Lambda_3\Lambda_2\Lambda_1$; where Λ_1 is a boost by β to the incident particle's rest frame, Λ_2 is a rotation by ψ to put the particle momentum along the z axis, and Λ_3 is a pure boost by β' along the z axis to achieve the center-of-mass frame. With these definitions, $\cos\psi=(\beta-\beta_j\cos\alpha)/v_{\rm rel}$ and $\beta'=\beta_2\gamma\mathcal{E}_j(1-\beta\beta_j\cos\alpha)/[M+\gamma\mathcal{E}_j(1-\beta\beta_j\cos\alpha)]$ where M is the mass of the incident particle and β_2 is the velocity of the target particle in the rest frame of the incident particle, $\beta_2=v_{\rm rel}/(1-\beta\beta_j\cos\alpha)$.

In what follows, we drop the final-state occupation number $(1\mp n_{jf})$. When the incident particle is relativistic, the final energy of the target particle is almost always greater than T, so this is justified. When the incident particle is nonrelativistic, n_{jf} should be included. Omitting it leads to an error of at most order unity as long as the target particles are not strongly degenerate.

For an unpolarized target medium $d\sigma_j/d\Omega$ does not depend on ϕ, so upon integration over $d\Omega$, the term proportional to $\cos\phi$ in Eq. (A2) drops out. Equation (A1) may then be rewritten as

$$\frac{dE}{dt}=\sum_j \frac{g_j}{2\pi}\int n_j(\mathbf{k})\mathscr{E}_j I_j(k)k^2 dk \ ,$$

$$I_j(k)=\int \Delta_j \frac{d\sigma_j}{d\Omega}\sin\alpha\sin\theta\, d\alpha\, d\theta \ , \tag{A3}$$

$$\Delta_j = v_{\rm rel}\{\gamma^2\gamma'^2(1-\beta\beta_j\cos\alpha) \times[(1-\beta'\beta_2)(1-\beta\beta'\cos\psi) -(\beta'-\beta_2)(\beta'-\beta\cos\psi)\cos\theta]-1\} \ .$$

Equation (A3) is completely general. We now apply it to some specific cases. We begin by noting that at early times ($T\gtrsim 0.1$ MeV), stopping is dominated by scattering from electrons and positrons rather than photons, because Coulomb cross sections are much larger than Compton cross sections. At later times, photons dominate because the number density of photons is much greater than the number density of electrons, $n_e/n_\gamma \simeq \eta \simeq$ few $\times 10^{-10}$. We start with the case where the target particles are electrons. The cross section for elastic electron-hadron collisions may be written[58] in terms of the relativistic kinematic invariants s,t,u:

$$\frac{d\sigma}{dt}=\frac{\pi\alpha^2}{[s-(M+m_e)^2][s-(M-m_e)^2]}\frac{1}{t^2}\frac{1}{(1-t/4m_e^2)} \times\left[F_e^2[(s-u)^2+(4M^2-t)t] -\frac{t}{4M^2}F_m^2[(s-u)^2-(4M^2-t)(4m_e^2+t)]\right] , \tag{A4}$$

where the electromagnetic form factors are defined by

$$F_e=F_1+\frac{t}{4M^2}F_2, \quad F_m=F_1+F_2 \ .$$

At low energies ($t=0$), F_1 and F_2 are the charge and anomalous magnetic dipole moment of the hadron. For protons $F_2=1.79$, for neutrons $F_2=-1.91$ and for π's and K's, $F_2=0$. In terms of $d\sigma/dt$ the center-of-mass cross section is $d\sigma/d\Omega=-(p^2/\pi)d\sigma/dt$ where p is the center-of-mass momentum: $p=\beta'\gamma' M$ for hadron mass M.

Equations (A3) and (A4) yield a complicated expression that is clearer with a few simplifying approximations. First, the maximum temperature for our purposes is about 1 MeV. Therefore, in the incident particles rest frame, the energy of the electron is of order $\gamma\times$ (1 MeV). This quantity is almost always less than M, so we may expand in terms of the parameter $x\equiv\gamma\mathscr{E}/M$. For charged particles the cross section reduces to

$$\frac{d\sigma}{d\Omega_{\rm ch}}\simeq\frac{\alpha^2}{M^2x^2}\frac{1-\frac{1}{2}\beta_2^2(1-\cos\theta)}{\beta_2^4(1-\beta\beta_j\cos\alpha)^2(1-\cos\theta)^2} \tag{A5a}$$

and for neutrals

$$\frac{d\sigma}{d\Omega_{\rm nc}}\simeq\frac{\alpha^2F_2^2}{2M^2}\frac{1+\frac{1}{2}\beta_2^2(1-\cos\theta)}{\beta_2^2(1-\cos\theta)} \ . \tag{A5b}$$

Second, we keep the leading terms for Δ in the relativistic and nonrelativistic regimes. When the incident particle is relativistic $\gamma^2\gg 1$, $\beta\simeq 1$, and $\beta_2\cos\psi\simeq 1$; so

$$\Delta_{\rm rel}\simeq\gamma^2(1-\beta_j\cos\alpha)^2(1-\cos\theta) \ . \tag{A6a}$$

In the nonrelativistic regime, $\beta\ll 1$, $\gamma^2\simeq 1+\beta^2$ and

$$\Delta_{\rm nrel}\simeq(\beta^2-\beta\beta_j\cos\alpha)(\beta_j-\beta\cos\alpha)(1-\cos\theta) \ . \tag{A6b}$$

It is now straightforward to calculate I in the four cases of interest:

$$I_{\rm ch,rel}\simeq\frac{2\alpha^2\Lambda}{\mathscr{E}_j^2} \ , \tag{A7a}$$

$$I_{\rm nc,rel}\simeq\frac{3\alpha^2F_2^2\gamma^2}{M^2}(1+\beta_j^2/3) \ , \tag{A7b}$$

$$I_{\rm ch,nrel}\simeq\frac{4\alpha^2\beta^2\Lambda}{3\mathscr{E}_j^2\beta_j} \ , \tag{A7c}$$

$$I_{\rm nc,nrel}\simeq\frac{4\alpha^2F_2^2\beta^2}{3M^2}\left[2\beta_j+\frac{1}{\beta_j}\right] \ . \tag{A7d}$$

The parameter Λ in the charged-particle cases is of order 1 and is associated with the Coulomb divergence $\Lambda=\ln[2/(1-\cos\theta_{\rm min})]-1$, where $\theta_{\rm min}$ is determined by either the plasma frequency or the Debye screening length of the medium. For the nonrelativistic cases we assumed $\beta<\beta_j$ and calculated the integrals only to leading order in β. Our results for the nonrelativistic case may not seem familiar. This is because we have worked in the limit where the thermal velocity of the electrons is greater than the velocity of the slowing hadron $\beta<\beta_j$. In the other limit, $\beta>\beta_j$, almost every scattering event causes the hadron to lose energy. Furthermore, energy loss to plasma excitations is important. For our case, where $\beta<\beta_j$, neither of these statements is true. As a result, stopping power decreases with decreasing hadron velocity, whereas the better-known result has $dE/dt\sim 1/\beta$. For temperatures well below the electron mass, there will be a range of hadron energies where our formulas seriously underestimate the stopping power, but the final stage of thermalization is as described here. The crossover hadron energy is roughly $E\sim 5000TM$ where M is the mass of the hadron in GeV.

Next, we use Eq. (A7) to evaluate dE/dt for the various cases. For $T\gtrsim m_e$ we neglect the electron mass and with $g_e=4$ we find

$$\left.\frac{dE}{dt}\right|_{\rm ch,rel}=\frac{\pi\alpha^2}{3}\Lambda T^2 \ , \tag{A8}$$

and a stopping time τ to lose the relativistic energy

$$\tau_{\rm ch,rel}\simeq\frac{3E}{\pi\alpha^2\Lambda T^2}\simeq\frac{1.2\times10^{-14}}{\Lambda}\frac{(E/{\rm GeV})}{(T/{\rm MeV})^2}\ {\rm sec} \ . \tag{A9a}$$

Even for 100 GeV hadrons the stopping time is much shorter than a typical hadronic interaction time, for which Eq. (3.5) gives $\tau_{\rm int}\gtrsim 10^{-8}$ sec. Similarly, for neutrals we find

$$\tau_{\rm nc,rel}\simeq\frac{15M^3}{7\pi^3\alpha^2F_2^2T^4}$$
$$\simeq\frac{8.6\times10^{-10}}{F_2^2}\frac{(M/\text{GeV})^3}{(T/\text{MeV})^4}\ \text{sec}\ . \tag{A9b}$$

Again, as long as $T\gtrsim m_e$, neutrons stop. In the nonrelativistic regime, the kinetic energy decays away exponentially with a decay time

$$\tau_{\rm ch,nrel}\simeq\frac{9M}{4\pi\alpha^2\Lambda T^2}\simeq\frac{9\times10^{-15}}{\Lambda}\frac{(M/\text{GEV})}{(T/\text{MeV})^2}\ \text{sec} \tag{A9c}$$

and

$$\tau_{\rm nc,nrel}\simeq\frac{15M^3}{14\pi^3\alpha^2F_2^2T^4}$$
$$\simeq\frac{4.3\times10^{-10}}{F_2^2}\frac{(M/\text{GeV})^2}{(T/\text{MeV})^4}\ \text{sec}\ . \tag{A9d}$$

It should be clear that as long as electrons are thermally abundant, charged hadrons and neutral spin-$\frac{1}{2}$ baryons stop before they interact hadronically. As noted in Sec. III, we do not expect K_L to stop. At $t=0$, both F_1 and F_2 vanish, so the leading term in the cross section [Eq. (A4)] is proportional to $F_1^2\sim t^2$ which leads to a stopping power $\sim T^2/M^2$ weaker than for neutrons and a stopping time $\tau\gtrsim10^{-5}$ sec.

Next, we turn to the case where $T<m_e$. We note that mesons decay before they interact and begin by discussing the neutron stopping due to electron scattering when $T<m_e$. In the relativistic regime we use Eq. (A7b), but drop the $\beta_j^2/3$ term. The stopping power of neutrons is then

$$\frac{dE}{dt}=\frac{3\pi\alpha^2F_2^2E^2}{M^4}\rho_e\ , \tag{A10}$$

where

$$\rho_e=4(m_eT/2\pi)^{3/2}m_e\exp(-m_e/T) \tag{A10a}$$

is the mass density of electrons and positrons. Defining $x\equiv m_e/T$, the stopping time for relativistic neutrons is

$$\tau\simeq1.8\times10^{-8}x^{3/2}e^x\ \text{sec}\ . \tag{A11}$$

Neutrons stop before interacting hadronically with the medium when $\tau\Gamma_{\rm int}\simeq1$, where $\Gamma_{\rm int}$ is given in Eq. (3.5). Using $s_*=1$ and, for illustrative purposes, $\langle\sigma\beta\rangle=40$ mb and $\eta=5\times10^{-10}$ so that $\Gamma_{\rm int}$ in Eq. (3.5) is $\Gamma_{\rm int}=\Gamma_{\rm int}^*\equiv2\times10^7\times(T/1\ \text{MeV})^3\ \text{sec}^{-1}$, we find the electronic stopping is efficient if $4.5\times10^{-2}x^{-3/2}e^x<1$. For $x>5.8$ ($T\lesssim0.088$ MeV$=10^9$ K) relativistic neutrons do not stop by electron scattering. Rather, they stop by colliding with nuclei in the medium. Because of the exponential drop in electron number with temperature, this result is fairly insensitive to the uncertainties in the calculation. Once the neutrons become nonrelativistic, we must repeat the calculation using Eq. (A7d). The crossover point where Ne scattering is inefficient occurs at about the same point as for relativistic neutrons.

To be complete in our discussion of neutrons stopping at low T, we should consider $n\gamma$ scattering. The cross section for $n\gamma$ scattering[59] is

$$\frac{d\sigma}{d\Omega}=\frac{\alpha^2F_2^4}{8}\frac{\mathcal{E}^2}{M^4}(2+\sin^2\theta)\ , \tag{A12}$$

where here $\mathcal{E}$ is the photon energy. This cross section is smaller by $\sim T^2/M^2$ than ne scattering so the stopping power is down by $\sim10^{-8}$ at $T\sim0.1$ MeV. Specifically,

$$\frac{dE}{dt}=\frac{640\zeta(6)}{3\pi}\frac{\alpha^2F_2^4\gamma^2T^6}{M^4}\ , \tag{A13}$$

where ζ is the Riemann zeta function. Equation (A13) gives a stopping time due to photons, τ_γ:

$$\tau_\gamma=9.6\times10^{-6}(T/\text{MeV})^{-6}\ \text{sec}\ . \tag{A14}$$

Stopping due to photons becomes less important than nuclear interactions when $\tau_\gamma\gtrsim1$ sec. Using Eq. (3.5) again, we find $\tau_\gamma\Gamma_{\rm int}^*=1.9\times10^2(T/\text{MeV})^{-3}$. By the time electron stopping is unimportant at $T\simeq0.1$ MeV, photon stopping is $\sim10^{-5}$ of nuclear stopping.

Lastly, we consider the stopping of protons for $T<m_e$, beginning with Compton scattering. The low-energy cross section is

$$\frac{d\sigma}{d\Omega}=\frac{2\alpha^2}{3M^2}\ , \tag{A15}$$

which, for relativistic protons, gives

$$\frac{dE}{dt}=\frac{32\pi^3}{135}\frac{\alpha^2\gamma^2}{m^2}T^4\ , \tag{A16}$$

$$\tau=1.4\times10^{-9}(T/\text{MeV})^{-4}\ \text{sec}\ . \tag{A17}$$

Nuclear interactions become important when $\tau\Gamma_{\rm int}^*\simeq2.8\times10^{-2}(T/\text{MeV})^{-1}$ is about 1, or at $T\simeq2.8\times10^{-2}$ MeV. Even though $\Gamma_{\rm int}^*\tau_\gamma>1$, since $dE/dt\sim E^2$ in Eq. (A16), for very-high-energy protons, Compton scattering will dominate until $E<E_c=0.028\ \text{MeV}/T\times\Gamma_{\rm int}/\Gamma_{\rm int}^*$ GeV. For nonrelativistic protons, replace γ^2 by β^2 in Eq. (A16). Since $\Gamma_{\rm int}^*\tau>1$, Compton scattering cannot prevent low-energy hadronic interactions when $T\lesssim0.03$ MeV.

Coulomb scattering is more involved. In the relativistic regime using Eq. (A7a) in Eq. (A3) leads to

$$\frac{dE}{dt}=\frac{2\pi\alpha^2\Lambda}{m_e^2}\rho_e \tag{A18}$$

with ρ_e given in Eq. (A10a) until $T=m_e/26\simeq0.04m_e$ when positrons freeze-out, and by $\rho_e=m_e\eta_en_\gamma$ for lower temperatures, where $\eta_e=\eta_B(1-Y/2)$. After positrons freeze-out this gives $\Gamma_{\rm int}^*\tau=160(E/1\ \text{GeV})(1-Y/2)/\Lambda$, and we see that Coulomb scattering is not very important. Before positrons freeze-out, one expects few hadronic interactions unless $\eta_e<10^{-7}$ which happens when $T<m_e/20$. Nonrelativistically, we consider two regimes. When the protons are fast, i.e., $\beta_p>\langle\beta_e\rangle$, the stopping power is given by

$$\frac{dE}{dt}=\frac{4\pi\alpha^2\Lambda}{\beta_pm_e^2}\rho_e\ , \tag{A19}$$

where the dominant contribution comes from plasma excitations.[60] After $\beta_p < \langle \beta_e \rangle$, slow protons are stopped primarily by two-body scattering. In this case we use Eq. (A7b) and find

$$\frac{dE}{dt} = \frac{4\pi\alpha^2\beta_p^2\Lambda}{3m_e^2}\rho_e\left\langle\frac{1}{\beta_e}\right\rangle . \tag{A20}$$

After freeze-out, $\Gamma^*_{\rm int}\tau = 1.4\times10^2(1-Y/2)/\Lambda$, which provides similar conditions for the importance of Coulombic scattering as in the relativistic case.

There is a substantial numerical difference between Eqs. (A19) and (A20). This leads us to suspect that during the transition, where the protons are slowing to velocities less than those of thermal electrons, the stopping power has not been calculated very accurately. The transition energy is $E\sim5000TA$ where A is the atomic number of the nucleus (we generalize to nuclei heavier than protons). The implication is that at $t\sim10^4$ sec, $T\sim0.01$ MeV, the final stages of stopping ($E<50$ MeV) will be described by Eq. (A20). Stopping will be dominated by nuclear interactions. These energies are low enough that protons stopping via nuclear interactions will cause relatively little ^{4}He fission. However, the energies are high enough that deuterium, tritium, or ^{3}He having significant nuclear interactions will be likely to undergo fission, while stopping. The result is that around 10^4 sec any reaction products from ^{4}He fission (due to fast neutrons or antibaryons) may be totally disrupted into individual nucleons. At this point, deuterium formation is still fast enough to put most of that back into deuterium, although not much will be cooked into ^{4}He. By 10^5 sec it is much more difficult to anticipate what will happen. The transition between fast and slow nuclei happens at lower energies, and the efficiency for forming deuterium is not as high. We have not attempted to address this issue in this paper and refer the reader to DEHS for a detailed discussion.

We capitulate our discussion of stopping powers. For the mesons, whenever mesons may interact before decaying, they stop first. The only exception is K_L which interacts while it is relativistic. Protons stop very efficiently due to electrons or photons until $T\sim0.03$ MeV. After that, nuclear stopping becomes important. Neutrons stop via electron scattering until $T\sim0.09$ MeV after which nuclear stopping dominates. Whenever nuclear stopping is important the possibility of creating free neutrons via hadronic collisions must be considered.

[1]R. V. Wagoner, W. A. Fowler, and F. Hoyle, Astrophys. J. **148**, 3 (1967); R. V. Wagoner, Astrophys. J. Suppl. **18**, 247 (1969); Astrophys. J. **179**, 343 (1973).

[2]J. Yang, M. S. Turner, G. Steigman, D. N. Schramm, and K. A. Olive, Astrophys. J. **281**, 493 (1984).

[3]See, for example, J. S. Gallagher, in *Inner Space/Outer Space,* edited by E. W. Kolb, M. S. Turner, D. Lindley, K. A. Olive, and D. Seckel (University of Chicago Press, Chicago, 1986).

[4]J. H. Applegate and C. J. Hogan, Phys. Rev. D **31**, 3037 (1985); **34**, 1938(E) (1986); K. E. Sale and G. J. Matthews, Astrophys. J. **309**, L1 (1986); J. H. Applegate, C. J. Hogan, and R. J. Scherrer, Phys. Rev. D **35**, 1151 (1987).

[5]A. Yahil and G. Beaudet, Astrophys. J. **206**, 26 (1976); Y. David and H. Reeves, in *Physical Cosmology,* edited by R. Balian *et al.* (North-Holland, Amsterdam, 1980) p. 443; K. Freese, E. W. Kolb, and M. S. Turner, Phys. Rev. D **27**, 1689 (1983).

[6]E. W. Kolb and R. J. Scherrer, Phys. Rev. D **25**, 1481 (1982).

[7]R. J. Scherrer and M. S. Turner, Phys. Rev. D **31**, 681 (1985); Report No. FERMILAB-Pub-85/170-A, 1985 (unpublished); Report No. FERMILAB-Pub-87/99-A, 1987 (unpublished).

[8]J. Ellis, D. Nanopoulos, and S. Sarkar, Nucl. Phys. **B259**, 175 (1985); D. Lindley, Astrophys. J. **294**, 1 (1985); M. Kawasaki and K. Sato, Phys. Lett. B **189**, 23 (1987).

[9]R. Juszkiewicz, J. Silk, and A. Stebbins, Phys. Lett. **158B**, 463 (1985).

[10]P. Salati, P. Delbourgo-Salvador, and J. Audouze, Annecy Report No. LAPP-TH-148, 1986 (unpublished); A. Bouquet and P. Salati, Nucl. Phys. **B284**, 557 (1987).

[11]R. Dominguez-Tenreiro, Astrophys. J. **313**, 523 (1987).

[12]M. Yu. Khlopov and A. D. Linde, Phys. Lett. **138B**, 265 (1984); Yu. A. Batusov *et al.,* Lett. Nuovo Cimento **41**, 223 (1984); J. Audouze, D. Lindley, and J. Silk, Astrophys. J. Lett. **293**, 153 (1985); D. Lindley, Phys. Lett. B **171**, 235 (1986).

[13]L. J. Hall, in *Cosmology and Particle Physics,* proceedings of the Theoretical Workshop, Berkeley, California, 1986, edited by Ian Hinchliffe (World Scientific, Singapore, 1987); M. C. Bento, L. Hall, and G. G. Ross, Oxford University report, 1987 (unpublished).

[14]J. Bagger and S. Dimopoulos, Nucl. Phys. **B244**, 247 (1984); J. Bagger, S. Dimopoulos, E. Massó, and M. H. Reno, *ibid.* **B258**, 565 (1985); Phys. Rev. Lett. **54**, 2199 (1985).

[15]B. W. Lee and S. Weinberg, Phys. Rev. Lett. **39**, 165 (1977).

[16]R. Dominguez-Tenreiro and G. Yepes, Universidad Autónoma de Madrid report, 1987 (unpublished).

[17]S. Dimopoulos, R. Esmailzadeh, L. J. Hall, and G. D. Starkman, SLAC Report No. SLAC-PUB-4356, 1987 (unpublished).

[18]For a review, see D. Schramm and R. V. Wagoner, Annu. Rev. Nucl. Part. Sci. **27**, 37 (1977).

[19]Particle Data Group, M. Aquilar-Benitez *et al.,* Phys. Lett. **170B**, 1 (1986).

[20]We have used L. Kawano's version of the Wagoner code. Details about the solution of the coupled differential equations appear in Ref. 1. The program incorporates the new ^{7}Li reaction rates described in L. Kawano, D. Schramm, and G. Steigman, Ohio State University report, 1987 (unpublished).

[21]See, for example, G. Steigman, Annu. Rev. Nucl. Part. Sci. **29**, 313 (1979).

[22]A. M. Boesgaard and G. Steigman, Annu. Rev. Astron. Astrophys. **23**, 319 (1985); G. Steigman, K. A. Olive, D. N. Schramm, and M. S. Turner, Phys. Lett. B **176**, 33 (1986), and references therein.

[23]D. Kunth and W. L. W. Sargent, Astrophys. J. **273**, 81 (1983).

[24]Kawano, Schramm, and Steigman (Ref. 20), and references therein.

[25]In principle, ^{6}Li could also be used to constrain decaying X particles. At present, the experimental results for the ^{6}Li abundance are controversial, so we rely only on the ^{4}He, ^{3}He, and D limits for our presentation here. Additional con-

straints could only strengthen our bounds. Actually, a generic feature of our calculation is that the ratio $X_{^6\mathrm{Li}}/X_{^7\mathrm{Li}} \ll 1$, as in the standard BBN scenario.

[26]Let us assume that each antinucleon annihilates on ^{4}He with probability $\frac{1}{4}$ and releases 1.5 neutrons per annihilation. Further, assume that each fast neutron undergoes one collision with a ^{4}He nucleus while slowing from energies of a few GeV to less than 50 MeV and each of these collisions results in two free neutrons. Finally, for simplicity, let all neutrons end up in deuterium. Then for each injected neutron, we get the initial neutron, two neutrons from the high-energy n^4He collision, and 0.75 neutrons from annihilation of antibaryons on ^{4}He. The result is 3.75 deuterons per neutron injected. DEHS (Ref. 17) have done a more detailed analysis of this process for the time range 10^5–10^6 sec and conclude that as many as five ^{4}He nuclei may be disrupted per injected neutron. Of course, at that time not all free neutrons end up as deuterium.

[27]L. D. Roper, R. M. Wright, and B. T. Feld, Phys. Rev. **138**, B190 (1965).

[28]B. H. Bransden and R. G. Moorhouse, *The Pion Nucleon System* (Princeton University Press, Princeton, NJ, 1973).

[29]A. D. Martin and G. G. Ross, Nucl. Phys. **B16**, 479 (1970).

[30]V. Flamino, W. G. Moorhead, D. R. O. Morrison, and N. Rivoire, Report No. CERN-HERA 83-02, 1983 (unpublished).

[31]T. Kalogeropoulos and G. S. Tzanakos, Phys. Rev. D **22**, 2585 (1980).

[32]A. H. Mueller, Phys. Lett. **104B**, 161 (1981).

[33]R. Felst, in *Lepton and Photon Interactions at High Energies*, proceedings of the 10th International Symposium, Bonn, 1981, edited by W. Pfeil (Bonn University, Physics Institute, Bonn, Germany, 1981), p. 52; S. L. Wu, Phys. Rept. **107**, 59 (1984).

[34]M. Shapiro, Ph.D. thesis, Lawrence Berkeley Laboratory Report No. LBL-18820, 1984.

[35]A similar effect is considered in Refs. 11 and 16, however, our numerical conclusions differ for a variety of reasons. See Sec. IV B 1.

[36]See, however, Ref. 17.

[37]H. Pagels and J. Primack, Phys. Rev. Lett. **48**, 223 (1982); S. Weinberg, *ibid.* **48**, 1303 (1982).

[38]D. Nanopoulos, K. Olive, and M. Srednicki, Phys. Lett. **127B**, 30 (1983).

[39]J. Ellis, J. Kim, and D. Nanopoulos, Phys. Lett. **145B**, 181 (1984).

[40]L. Krauss, Nucl. Phys. **B227**, 556 (1983). This value of $\tau_{\tilde{G}}$ is larger than that given in Ref. 39 by a factor of $\pi/2$.

[41]The results in Ref. 9 are comparable to those of Ellis, Nanopoulos, and Sarkar in Ref. 8 but markedly stronger than those of Kawasaki and Sato in Ref. 8.

[42]We note that there is apparently a difference between our computer code and that of Ref. 11, as we find $Y=0.257$ for $\eta=7\times10^{-9}$, $\tau_{1/2}=10.4$ min, and $N_\nu=2$ with no X decays, whereas Dominguez-Tenreiro apparently finds $Y\leq0.25$.

[43]F. Zwirner, Phys. Lett. **132B**, 103 (1983); L. J. Hall and M. Suzuki, Nucl. Phys. **B231**, 419 (1984); I-Hsiu Lee, *ibid.* **B246**, 120 (1984); R. Barbieri and A. Masiero, *ibid.* **B267**, 679 (1985); S. Dawson, *ibid.* **B261**, 297 (1985).

[44]C. S. Aulakh and R. N. Mohapatra, Phys. Lett. **119B**, 136 (1982); G. Ross and J. Valle, *ibid.* **151B**, 375 (1985); J. Ellis, G. Gelmini, C. Jarlskog, G. G. Ross, and J. W. F. Valle, *ibid.* **150B**, 142 (1985); Dawson (Ref. 43); R. N. Mohapatra, Phys. Rev. D **34**, 3457 (1986).

[45]H. Goldberg, Phys. Rev. Lett. **50**, 1419 (1983); J. Ellis, J. S. Hagelin, D. V. Nanopoulos, K. A. Olive, and M. Srednicki, Nucl. Phys. **B238**, 453 (1984).

[46]We use the notation (without generation labels) of Dawson (Ref. 43).

[47]See, for example, B. Greene, K. Kirklin, P. Miron, and G. G. Ross, Phys. Lett. B **180**, 69 (1986).

[48]P. F. Smith, J. R. J. Bennett, G. J. Homer, J. D. Lewin, H. E. Halford, and W. A. Smith, Nucl. Phys. **B206**, 333 (1982).

[49]E. B. Norman, S. B. Gazes, and D. A. Bennett, LBL report, 1986 (unpublished).

[50]For a review, see E. W. Kolb and M. S. Turner, Annu. Rev. Nucl. Part. Sci. **33**, 645 (1983).

[51]K. Griest and D. Seckel, Nucl. Phys. **B283**, 681 (1987).

[52]E. W. Kolb and K. A. Olive, Phys. Rev. D **33**, 1202 (1986); **34**, 2531 (1986).

[53]P. W. Hodge, Annu. Rev. Astron. Astrophys. **19**, 357 (1981).

[54]On the basis of cosmological arguments and accelerator experiments, $N_\nu=2$ means that the mass of the τ neutrino is between 20–70 MeV. See Refs. 6 and 19.

[55]G. Blumenthal, A. Dekel, and J. Primack, SCIPP Report No. 87/81, 1987 (unpublished).

[56]D. A. Dicus, E. W. Kolb, A. M. Gleeson, E. C. G. Sudarshan, V. T. Teplitz, and M. S. Turner, Phys. Rev. D **26**, 2694 (1982).

[57]Steigman, Olive, Schramm, and Turner (Ref. 22).

[58]V. B. Berestetskii, E. M. Lifshitz, and L. P. Pitaevskii, *Quantum Electrodynamics* (Pergamon, London, 1982), p. 630.

[59]Berestetskii, Lifshitz, and Pitaevskii, *Quantum Electrodynamics* (Ref. 58), p. 638.

[60]J. D. Jackson, *Classical Electrodynamics* (Wiley, New York, 1975), p. 643.